

The Delicate Bistability of CaMKII

P. J. Michalski*

Richard D. Berlin Center for Cell Analysis and Modeling, University of Connecticut Health Center, Farmington, Connecticut

ABSTRACT Calcium/calmodulin-dependent protein kinase II (CaMKII) is a synaptic, autophosphorylating kinase that is essential for learning and memory. Previous models have suggested that CaMKII functions as a bistable switch that could be the molecular correlate of long-term memory, but experiments have failed to validate these predictions. These models involved significant approximations to overcome the combinatorial complexity inherent in a multisubunit, multistate system. Here, we develop a stochastic particle-based model of CaMKII activation and dynamics that overcomes combinatorial complexity without significant approximations. We report four major findings. First, the CaMKII model system is never bistable at resting calcium concentrations, which suggests that CaMKII activity does not function as the biochemical switch underlying long-term memory. Second, the steady-state activation curves are either laserlike or steplike. Both are characterized by a well-defined threshold for activation, which suggests that thresholding is a robust feature of this system. Third, transiently activated CaMKII can maintain its activity over the time course of many experiments, and such slow deactivation may account for the few reports of bistability in the literature. And fourth, under *in vivo* conditions, increases in phosphatase activity can increase CaMKII activity. This is a surprising and counterintuitive effect, as dephosphorylation is generally associated with CaMKII deactivation.

INTRODUCTION

The processes of learning and memory require long-term changes in the neural network to assimilate and store new information (1). At the cellular level, these changes are thought to include the formation, elimination, and modification of synapses, all of which fall under the general category of synaptic plasticity (2–4). Two of the most well studied examples of synaptic plasticity are long-term potentiation (LTP), a persistent increase in the efficacy of synaptic transmission (5), and its converse, long-term depression (LTD), a persistent decrease in the efficacy of synaptic transmission (6). At the molecular level, LTP is usually characterized by an increase in the size of dendritic spines (7) and an increase in the number of synaptic AMPA receptors (AMPA receptors) (8), whereas LTD is usually characterized by the opposite changes. LTP and LTD are controlled by a vast signaling network whose functional properties are still being elucidated (9). In particular, it is at present unknown which signaling molecule(s) undergoes permanent changes leading to the persistent changes in spine size and synaptic AMPAR numbers.

Several possible molecular mechanisms have been proposed to account for the permanent changes at the synapse, including changes in local transcription rates, changes in kinase/phosphatase activities, changes in the organization of scaffolding proteins, and changes in the localization/aggregation of certain proteins (10,11). The common requirement for any molecular correlate of long-term memory is that it must be stable in the presence of protein turnover (12), because protein turnover times are on the order of seconds to a few weeks, whereas long-term memories can

last for a lifetime. A leading candidate for a permanent molecular switch that is stable to protein turnover is a system composed of an autophosphorylating kinase coupled to a phosphatase (13). Under certain conditions, such a system can form a bistable switch, where at basal conditions states of low and high kinase activity are both stable, and the current activity state depends on the history of the system (13).

Calcium/calmodulin-dependent protein kinase II (CaMKII) is an autophosphorylating kinase (14,15) that constitutes up to 2% of total protein in certain regions of the brain and is highly enriched at synapses (16). CaMKII is activated by calcium-saturated calmodulin (CaM) (17), and once activated, it can autophosphorylate at T286 (18). Once phosphorylated at this site, CaMKII is autonomously active, that is, active even in the absence of Ca^{2+} /CaM (19). This site can be dephosphorylated by several synaptically localized protein phosphatases, including PP1 and PP2A (20). This CaMKII-phosphatase system satisfies the minimum requirements of the autophosphorylating kinase-phosphatase system described above, and it is therefore possible that a bistable CaMKII switch forms the molecular basis of synaptic plasticity and long-term memory (21).

Indeed, there is strong evidence that CaMKII plays a central role in synaptic plasticity and memory. CaMKII activation is necessary (22,23) and sufficient (24,25) for hippocampal NMDAR-dependent LTP, and CaMKII knockout (26–28) and knockdown (29) mice show severe deficits in several learning tasks. Phosphorylation of T286 is significantly increased after LTP induction (30–33), and CaMKII autonomy is required for LTP induction (34,35) and normal learning and memory (36). However, investigations of persistent autonomous activity during LTP have given mixed results. Early studies showed a sustained

Submitted February 27, 2013, and accepted for publication June 25, 2013.

*Correspondence: michalski@uchc.edu

Editor: Dennis Bray.

© 2013 by the Biophysical Society
0006-3495/13/08/0794/13 \$2.00

<http://dx.doi.org/10.1016/j.bpj.2013.06.038>



increase in autonomous activity after LTP induction (37,38) and suggested that LTP maintenance requires autonomous activity (39,40). More recent work showed that although LTP induction indeed generates persistent T286 phosphorylation, it only transiently increases CaMKII autonomy (41), which suggests the involvement of additional deactivation mechanisms. In addition, many groups have shown that autonomy is required for LTP induction but not LTP maintenance (42–45). An in vitro study of the CaMKII-PP1 system found no evidence of bistability (46), but it is possible that the authors did not use large enough CaMKII concentrations to observe potential bistability.

The synaptic activity of CaMKII is regulated by a large biochemical signaling network with contributions from both calcium and cAMP pathways (9), and several groups have studied this network using computational models of varying complexity (47,48). In many cases, the models show that CaMKII activity is bistable at the basal state under a wide range of kinetic parameters and model assumptions (49–53). Although the models differ, a common requirement for bistability is that the phosphatase operate at saturation. In the postsynaptic density (PSD), the concentration of CaMKII subunits is 100–200 μM , whereas the Michaelis-Menten constants of the relevant phosphatases are on the order of 10 μM (46). Phosphatases should be saturated in such a situation, and thus the most important theoretical requirement for bistability is satisfied at the synapse.

Given the prevailing experimental evidence, it is reasonable to question the model predictions of robust bistability. In fact, modeling of CaMKII is difficult because of the combinatorial complexity that arises from its multisubunit holoenzyme structure (54), and most published models involve severe approximations that may invalidate their results. Here, we develop a detailed model of CaMKII activation that includes several physiologically relevant states not usually included in other models. We implement this model using particle-based, stochastic, network-free simulations that overcome combinatorial complexity and allow for an exact study of the system properties. Our major finding is that bistability is possible but physiologically irrelevant because it occurs over just a narrow range of calcium concentrations that are much higher than basal calcium levels. At low phosphatase concentrations, CaMKII activates through a laser transition, which differs from a more conventional Hill-type activation curve in that activity is nearly zero below a threshold, and above that threshold, the activity turns on in a linear fashion. Although the system is not bistable at basal conditions, autonomous activity decays very slowly after the system returns to resting calcium levels. Under physiological conditions, the decay times are on the order of several hours, which may account for the conflicting reports of in vivo bistability. Finally, we show that basal levels of inhibitory phosphorylation can greatly diminish the amount of autonomous activity generated by stimulation protocols and can change the func-

tion of phosphatases from CaMKII inhibitors to CaMKII activators.

MODEL

Calmodulin activation

Calmodulin (CaM) is a relatively small, dumb-bell-shaped calcium-binding protein that can bind four calcium ions, two at its N-lobe and two at its C-lobe (55). The lobes act independently of one another, but calcium binding at each lobe is a highly cooperative process (56–58). Models that take this lobe structure into account are required to study CaM dynamics over very short timescales (59,60), but for our purposes it is sufficient (61) to ignore the lobe structure and assume that CaM binds four calcium ions in a sequential manner. The five states of CaM are denoted CaM_i , $i = 0, \dots, 4$, where i indicates the number of bound calcium ions. The calcium binding kinetics are extremely fast, with some of the largest on and off rates ever measured (62), and we therefore assume that the calcium-binding reactions are in rapid equilibrium. This assumption is valid for all of the simulations presented here except for the LTP protocols discussed below, where we consider Ca^{2+} pulses at 100 Hz. In these cases, our assumption will tend to overestimate the amount of calcium-saturated CaM, but in that section our main focus will be on the kinetics of deactivation, which occurs on very long timescales where again the rapid equilibrium assumption is valid.

Using the fact that CaM is buffered in all of the situations studied here, we have

$$\text{CaM}_0 = \text{CaM}_{\text{tot}} \left(1 + \frac{\text{Ca}}{K_0} + \frac{\text{Ca}^2}{K_0 K_1} + \frac{\text{Ca}^3}{K_0 K_1 K_2} + \frac{\text{Ca}^4}{K_0 K_1 K_2 K_3} \right)^{-1}, \quad (1)$$

$$\text{CaM}_i = \left(\frac{\text{Ca}}{K_{i-1}} \right) \text{CaM}_{i-1}, \quad i = 1, \dots, 4$$

where Ca is the free Ca^{2+} concentration (assumed buffered), K_i is the dissociation constant for the reaction $\text{CaM}_i + \text{Ca}^{2+} \rightleftharpoons \text{CaM}_{i+1}$, and $\text{CaM}_{\text{tot}} = \sum \text{CaM}_i$ is the total, buffered concentration of cytosolic calmodulin (that is, not bound to CaMKII). The K_i values used here are listed in Table S1 in the Supporting Material.

CaMKII structure and states

A single CaMKII subunit is composed of an association domain, a linker region, a regulatory domain, and a kinase domain (63), as depicted in Fig. 1 A. CaMKII subunits cluster together through their association domains to form a 12-subunit holoenzyme, shown schematically in Fig. 1 B, with the association domains forming a central hub and the kinase domains protruding in a gear shape (64–66). In its initial inactive form, D_{aut} , the CaMKII subunit is autoinhibited because the regulatory domain blocks the ATP and substrate binding sites on the kinase domain (67). An active form, C_{u} , is generated when fully saturated CaM (CaM_4) binds to and displaces the regulatory domain, which exposes the ATP and substrate sites (67). This also exposes T286 in the regulatory domain, which can be phosphorylated by a neighboring active subunit (68–70), giving state C_{p} . Phosphorylation of T286 prevents the regulatory domain from fully inhibiting the kinase domain, even in the absence of $\text{Ca}^{2+}/\text{CaM}$ and thus generates a Ca^{2+} -independent (autonomous) subunit, D_{pu} , whose activity is usually 20–80% of CaM-stimulated activity (71). Dissociation of CaM exposes T305/T306, which can be autophosphorylated through an intrasubunit reaction (69). Phosphorylation at these sites prevents CaM binding and locks the subunit in a partially active state, D_{pp} (72,73). In addition, the initial autoinhibited subunit can undergo a Ca^{2+} -independent basal

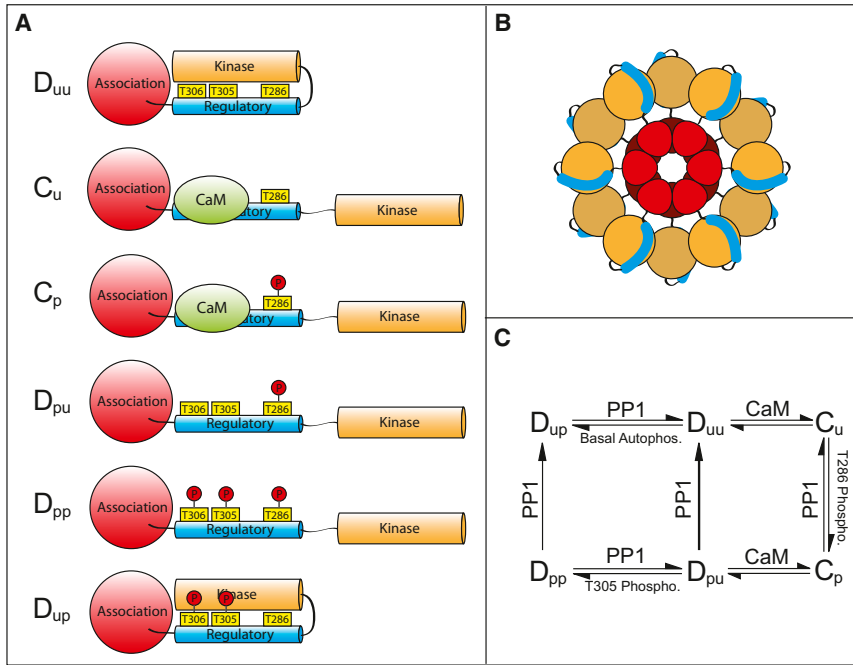


FIGURE 1 Model states and reactions. (A) A CaMKII subunit can exist in one of six states depending on CaM binding and phosphorylation at several sites. The six states are as follows: D_{uu} , autoinhibited; C_u , CaM-bound, unphosphorylated; C_p , CaM-bound, phosphorylated on T286; D_{pu} , phosphorylated on T286, T305, and T306; and D_{uu} , phosphorylated on T305 and T306. States D_{uu} and D_{up} are inactive; the other states have varying activity levels. (B) A schematic view of the dodecameric CaMKII holoenzyme. Association domains are shown in red, regulatory domains in blue, and kinase domains in orange. (C) Reaction diagram describing conversion between the six states of CaMKII. See the text for details.

autophosphorylation on T305/T306 (74). The resulting state, D_{up} , must be dephosphorylated before activation by CaM, and we will refer to this state as the doubly inhibited state. Basal autophosphorylation is very slow in vitro (74) but may be accelerated by some scaffolding proteins in vivo (75). For simplicity, in our model we treat the double phosphorylation event on T305/T306 as a single event on T305.

CaMKII reactions

Fig. 1 C shows a schematic representation of the CaMKII reaction diagram. The reactions can be loosely grouped into three categories.

Calmodulin binding

Although partially saturated CaM can bind to CaMKII, it only weakly stimulates kinase activity compared to fully saturated CaM (76,77). Thus, we only allow fully saturated CaM (CaM_4) to bind to and activate CaMKII. In Pepke et al. (60), it was shown that this assumption overestimates the amount of CaMKII activation on short timescales compared to models that allow binding by partially saturated CaM. The timescales considered here are long enough so that our assumption is valid, except during the rapid calcium pulses considered during LTP and LTD protocols. However, as mentioned above, our primary interest in these cases is the kinetics of CaMKII deactivation, which occurs over timescales long enough for our assumption to be valid.

CaM binding kinetics strongly depend on the phosphorylation state of T286 (78,79). We therefore introduce two on rates, $k_{on,u}$ and $k_{on,p}$, to describe binding to the unphosphorylated and phosphorylated T286 species, respectively. We allow CaM dissociation to proceed through one of two pathways: either CaM_4 directly dissociates from CaMKII, or CaM loses two Ca^{2+} and then rapidly dissociates as CaM_2 . As we do not include states with partially saturated CaM bound to CaMKII, this second dissociation pathway is described by a calcium-dependent off rate for CaM_4 . The full CaM dissociation rate is given by

$$k_{off,i} = k_{off,i}^{(1)} + \frac{k_{off,i}^{(2)}}{1 + (\text{Ca}/K_{\text{Ca},i})^2}, \quad (2)$$

where $i = u$ or $i = p$, depending on the phosphorylation state of T286, $k_{off,i}^{(1)}$ is the dissociation rate of fully saturated CaM, $k_{off,i}^{(2)}$ is the maximal effective dissociation rate for the Ca^{2+} -dependent dissociation pathway, and $K_{\text{Ca},i}$ is the calcium concentration giving the half-maximal calcium-dependent dissociation rate. The values for the CaM-CaMKII binding rates are listed in Table S1.

Recent experimental evidence suggests that CaMKII subunits in the holoenzyme pair up through their regulatory domains (80,81) and that this interaction leads to positive cooperativity in CaM binding (82). It is difficult to reconcile this evidence of positive cooperativity with previous studies that showed no cooperativity in CaM binding (83,46). Therefore, we have not included such an interaction in the model considered in the main text. In the Supporting Material, we do consider a model with cooperative CaM binding and compare it to the results shown below for the noncooperative model. We find that cooperative CaM binding has a negligible effect on CaMKII activation and does not change any of our major conclusions, which justifies its omission from the main model considered here. See the Supporting Material for a full description of the cooperative CaM binding mode.

Autophosphorylation

Phosphorylation of T286 is an intersubunit reaction whereby an active subunit phosphorylates a neighboring, CaM-bound subunit. We make the common assumption (61,84) that phosphorylation proceeds in a unidirectional manner around the holoenzyme. Autophosphorylation is a first-order reaction that may occur at different rates depending on the state of the kinase subunit (the substrate subunit is always C_u) (84). We therefore introduce four autophosphorylation rates depending on the state of the kinase subunit: r_1 for C_u , r_2 for C_p , r_3 for D_{pu} , and r_4 for D_{pp} . Based on activities toward exogenous substrates, we assume that $r_2 = r_1$ (85), $r_3 = 0.8r_1$ (83), and $r_4 = r_3$ (73). This leaves r_1 as the only free autophosphorylation rate.

Phosphorylation of T305 is an intrasubunit reaction that can occur in one of two first-order reactions. The autoinhibited subunit can directly phosphorylate T305 with a slow basal rate, r_b . Alternatively, the autonomously active subunit, D_{pu} , rapidly phosphorylates T305 with a rate r_{305} . The values for all autophosphorylation rates are listed in Table S1.

Dephosphorylation

The phosphatases PP1 and PP2A dephosphorylate T286 and T305 *in vivo*, with most PP1 activity in the PSD and most PP2A activity in the cytosol (20). Here, we will use PP1 to denote all phosphatase activity. Dephosphorylation proceeds through a standard irreversible Michaelis-Menten reaction with reaction flux

$$J_{X,PP1} = \frac{n_X k_c PP1_{act} X}{K_m + \Sigma_p}, \quad (3)$$

where X is the species being dephosphorylated, n_X is the number of phosphorylated residues on X , k_c is the catalytic rate constant, K_m is the Michaelis-Menten constant, $PP1_{act}$ is the concentration of active PP1, and $\Sigma_p = C_p + D_{pu} + D_{up} + 2D_{pp}$ is the total concentration of phosphorylated residues. We assume that PP1 has equal activity toward T286 and T305 (same k_c and K_m), and we assume that there is no preference for the order in which these residues are dephosphorylated. Parameter values are listed in Table S2.

PP1 regulation

PP1 is deactivated by binding to phosphorylated inhibitor-1 (I1) (86,87). I1 is dephosphorylated by the phosphatase calcineurin (CaN) (86), whose activity is regulated by calcium and calcium-bound CaM (88). I1 is phosphorylated by protein kinase A (PKA) (86), whose activity is stimulated by cAMP (89). As the levels of cAMP are controlled (at least partially) by CaM-activated adenylyl cyclases (90,91) and CaM-activated phosphodiesterases (92), the activity of PKA can be treated as a function of CaM. A schematic diagram of this regulatory network is shown in Fig. S1. Following the methods of Zhabotinsky (51) and Graupner and Brunel (52), we assume that CaN and PKA are in rapid equilibrium with CaM and write their activities as Hill functions:

$$\begin{aligned} V_{CaN} &= k_{CaN}^{(0)} + \frac{k_{CaN} (CaM_4 / K_{CaN})^{n_{CaN}}}{1 + (CaM_4 / K_{CaN})^{n_{CaN}}}, \\ V_{PKA} &= k_{PKA}^{(0)} + \frac{k_{PKA} (CaM_4 / K_{PKA})^{n_{PKA}}}{1 + (CaM_4 / K_{PKA})^{n_{PKA}}}, \end{aligned} \quad (4)$$

where $k_{CaN}^{(0)}$ is the basal activity of CaN, k_{CaN} is the maximum CaM-stimulated CaN activity, K_{CaN} is the CaM_4 concentration at half-maximal CaN activity, and n_{CaN} is the Hill exponent. The symbols with subscript PKA have the same meanings but apply to PKA activity.

Although the concentration of active PP1 is a function of calcium, it is not necessary to include this dependence when studying the steady-state activation of CaMKII. As pointed out in Graupner and Brunel (52), it is sufficient to determine steady-state activation as a function of calcium for various concentrations of PP1 and then combine these curves to make a phase diagram depicting CaMKII activity as a function of calcium and PP1. Assuming a specific functional form for steady-state active PP1 as a function of calcium then picks out a particular curve in this phase diagram.

For studies of the system dynamics the calcium dependence of PP1 activity must be included in the simulation because both active PP1 and I1 are dynamic variables. The concentrations of these evolve according to

$$\begin{aligned} \frac{dI1_p}{dt} &= -k_{on,PP1} I1_p P_{act} + k_{off,PP1} P_{inact} - V_{CaN} I1_p + V_{PKA} I1_{tot}, \\ \frac{dP_{act}}{dt} &= -k_{on,PP1} I1_p P_{act} + k_{off,PP1} P_{inact}, \end{aligned} \quad (5)$$

where $I1_p$ is the concentration of phosphorylated I1, $I1_{tot}$ is the total cytosolic concentration of unphosphorylated I1 (assumed buffered), P_{act} is the

concentration of active PP1, P_{inact} is the concentration of inactive PP1, and $P_{tot} = P_{act} + P_{inact}$ is the total concentration of PP1.

Modeling platforms

It is not practical to implement the model described above using conventional deterministic simulations based on ordinary differential equations, because an exact implementation of the multistate, multisubunit holoenzyme would require a network of thousands of species and reactions (54). Such combinatorial complexity can be overcome by using a particle-based stochastic simulation, an approach frequently called network-free modeling because there is no need to enumerate the entire reaction network before the simulation (93). Instead, the simulation keeps track of the exact state of each subunit in every holoenzyme, and different holoenzyme configurations arise naturally as the system evolves. Reaction probabilities are calculated for each individual subunit, and the system is updated according to Gillespie's exact stochastic simulation algorithm (SSA) (94). We implemented the model using a custom Java program, which is described in the Supporting Material and is available upon request.

RESULTS

Model validation

We validated the dynamic properties of the model by reproducing the experimental results of De Koninck and Schulman (83), where CaMKII activation was shown to be frequency dependent. We validated the steady-state properties of the model by reproducing the results of Bradshaw et al. (46), which explored steady-state CaMKII activation as a function of calcium and PP1. The comparisons to these two experiments are discussed in the Supporting Material and shown in Figs. S2 and S3. In both cases, the model results are in excellent qualitative and quantitative agreement with the experimental results. We conclude that the model accurately captures CaMKII dynamics and steady-state activation.

Steady-state solutions and bistability

To investigate steady-state solutions and search for regions of bistability, we began with a system with no activity ($Ca^{2+} = 0 \mu M$) and increased calcium in increments. At each increment, the system is run to steady state, and then Ca^{2+} is increased again. We continue in this manner until the system plateaus at a high steady-state activity. We then run this process in reverse, beginning with the high-activity steady state and decrementing Ca^{2+} until we again reach the system with no activity. If, for a certain Ca^{2+} level, the steady-state activity during the decrementing phase is different from that during the incrementing phase, then we conclude that the system exhibits bistability at that Ca^{2+} level. An example of this process is shown in Fig. 2A, where we show the time course of CaMKII activity during the entire process of increasing and decreasing Ca^{2+} . Fig. 2B shows the average steady-state activity as a function of Ca^{2+} for this same simulation, with the data points color-coded to indicate the activity values as we increased and

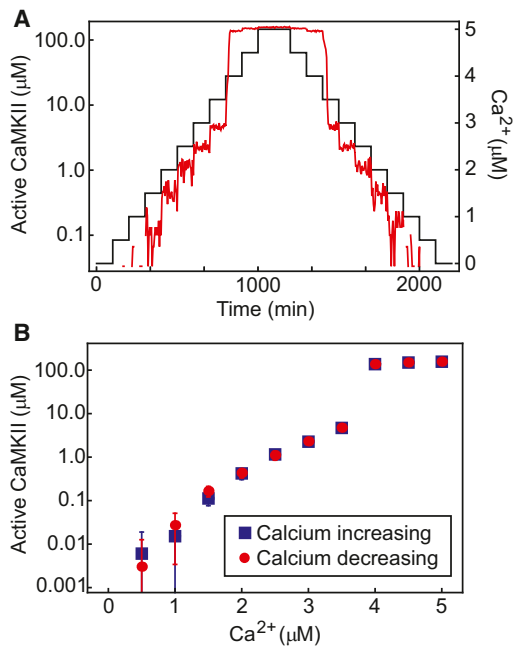


FIGURE 2 Illustrative example of the incremental calcium scan used to search for bistability. (A) A plot of the concentrations of Ca^{2+} (black) and active subunits (red) as a function of time. Here, calcium is increased in increments of $0.5 \mu\text{M}$ every 100 min, which is about twice as long as required to reach steady state under these conditions. (B) A plot of steady-state CaMKII activity as a function of Ca^{2+} , as derived from the time course in A. The system equilibrates to the same activity level whether calcium is increasing or decreasing, and thus there is no evidence of bistability under these conditions.

decreased calcium. Here, the system evolves to the same level of activity regardless of the direction of calcium changes, and thus we conclude that the system does not exhibit bistability for the chosen parameters.

We used the process described above to generate steady-state activity curves for several values of r_1 , CaM, and PP1 (CaM_{tot} = 0.1, 1.0, 10.0, and 100.0 μM , r_1 = 1.0, 10.0, and 100.0 s^{-1} , and PP1 = 0.01–50.0 μM to cover a broad range that is guaranteed to contain the *in vivo* concentration, estimated at 0.1–1.0 μM (51)). The range of parameters was chosen to cover all relevant physiological concentrations and rates, and also samples some extreme cases. Fig. 3 shows typical steady-state activity curves obtained with 0.1 μM CaM and the slower set of phosphorylation rates (r_1 = 1 s^{-1} , etc.). Results for other combinations of CaM concentrations and autophosphorylation rates are shown in Figs. S4–S11. Each curve in Fig. 3 shows the steady-state activity as a function of calcium for different concentrations of PP1, from very low PP1 (A) to very high PP1 (L). At low PP1, there is no indication of bistability, but nor does the system respond in a simple Hill-like fashion. Instead, the activation curve resembles an imperfect transcritical bifurcation (also called a laser transition), where the activity remains very low until calcium increases above a threshold, at which point the system activity increases in a linear fashion

(linearity does not continue indefinitely, because the activity must saturate). As PP1 increases, the slope of the linear activation region increases (see Fig. 3, A–D). At a critical value of PP1, the slope diverges and a gap opens between regions of low and high activity, as shown in Fig. 3 E. As PP1 is further increased, the region of high activity continues to slide backward over the region of low activity (see Fig. 3, F and G), creating a region of bistability. As PP1 continues to increase, the region of bistability shifts to higher calcium concentrations and eventually begins to narrow (Fig. 3, H and I), and the low activity curve begins to bend more sharply upward and the high-activity curve bends more sharply downward, so that the gap between high and low activity regions decreases (Fig. 3, J and K). At a second critical value of PP1, these curves touch in a cusp (infinite slope) (Fig. 3 K is very close to this threshold). As PP1 continues to increase, the cusp is softened and the region of high activity occurs only at very high calcium concentrations. (In Fig. 3 J, high activity occurs only at much higher calcium concentrations than are shown. See, for example, Fig. S5, J–L, for plots with a softened cusp.)

This general trend is observed in all of our simulations. Changes in CaM or the phosphorylation rates do not affect the overall qualitative behavior but do affect the values of specific features like the initial slope above threshold in the transcritical bifurcation and the width and location of the bistable region. For one parameter set, 10 μM CaM and r_0 = 1 s^{-1} (Fig. S7), a region of bistability was not observed, but it may be that in this case the width of the bistable region is smaller than the calcium increment.

Two important features should be noted: 1), the width of the bistable region is narrow (relative to the calcium concentrations at which it occurs); and 2), the bistable region never extends down to include the basal calcium concentration. The location of the bistable region is shifted to lower calcium as CaM and r_1 increase, but even at the highest, non-physiological values investigated here, bistability required $\text{Ca}^{2+} > 0.5 \mu\text{M}$ (see Fig. S11, G and H). Kinase activity always remains low at resting calcium, and there is no way for this system to act as a memory switch. The narrowness of the bistable regions suggests that bistability will be difficult to observe *in vitro*. Experimental data would likely show steplike behavior with very high Hill coefficients.

The location of the activation thresholds and narrow bistable regions depends most strongly on the autophosphorylation rates and on the binding affinities between calcium and CaM. Experimental estimates of the autophosphorylation rates vary by about an order of magnitude, from 1 s^{-1} to about 30 s^{-1} , and we had already varied these parameters. On the other hand, the calcium–CaM binding affinities are well determined under a variety of experimental conditions (57) and we treated these as fixed parameters. Nevertheless, it was of interest to determine the affinities required to produce bistable regions at basal calcium levels. To do so, we rescaled all four calcium–CaM dissociation

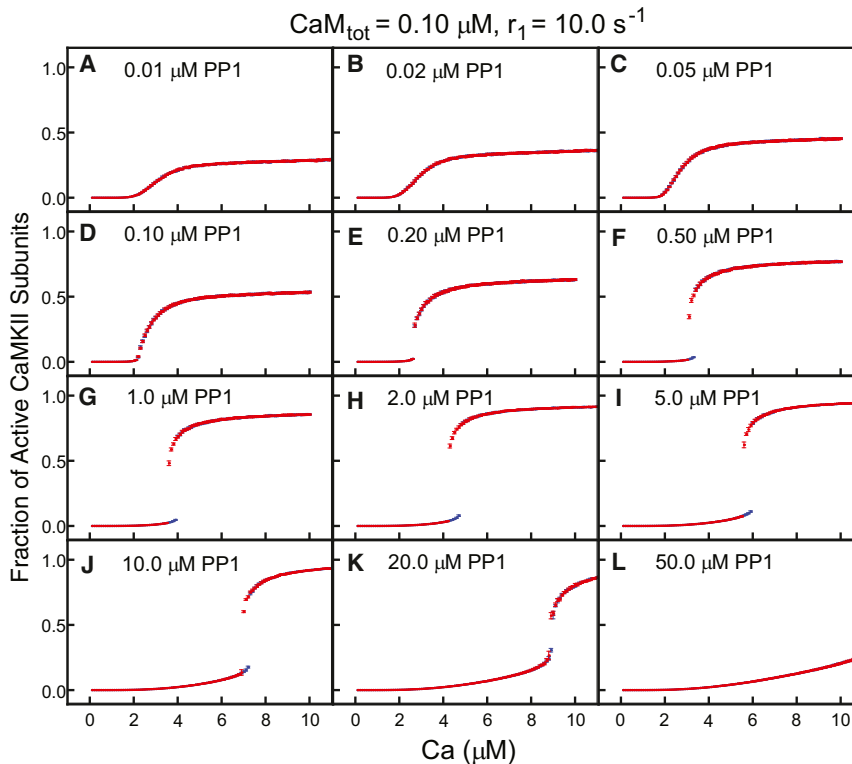


FIGURE 3 CaMKII activation curves. CaMKII activity is plotted as a function of Ca^{2+} for various concentrations of PP1, as labeled in the figures. As in Fig. 2 B, activity levels at increasing Ca^{2+} increments are shown in blue and those at decreasing Ca^{2+} increments are shown in red. Regions of bistability are easily identified by blue points at the edge of the lower activity curve. The interesting features and notable trends are discussed in the text. The simulations used standard parameters and $200 \mu\text{M}$ CaMKII.

constants by the same factor, $K_i \rightarrow K_i/\beta$, such that affinity increases with increasing β . We chose other parameters to provide the greatest chance of shifting the activity curves to lower thresholds: $r_1 = 100 \text{ s}^{-1}$ (three times the largest estimate) and $\text{CaM}_{\text{tot}} = 10 \mu\text{M}$ (large but plausible) or $100 \mu\text{M}$ (extreme). Figs. S12–S15 show a sample of the activation curves with $\beta = 2$ and 5 . We found that activation thresholds scaled nearly linearly with β . For example, with $\text{CaM}_{\text{tot}} = 100 \mu\text{M}$ and $\text{PP1} = 2 \mu\text{M}$, a tiny region of bistability occurs at $0.6 \mu\text{M}$ Ca^{2+} for $\beta = 1$ (Fig. S11 H), and is shifted to about $0.3 \mu\text{M}$ and about $0.13 \mu\text{M}$ for $\beta = 2$ (Fig. S14 H) and $\beta = 5$ (Fig. S15 H), respectively. However, the qualitative features of the activation curves did not change. It is important to note that regions of bistability remained very narrow and were frequently narrowed further or lost altogether (for example, compare Figs. S11 G and S14 G). Thus, even if calcium-CaM affinities are increased dramatically in vivo, this model predicts that no physiologically useful region of bistability will emerge.

In Fig. 4, we assemble the individual curves from Fig. 3 to form a phase diagram of CaMKII activity as a function of Ca^{2+} and PP1. The regions of bistability are too small to be of any interest on this scale, and we have made no attempt to show them in the phase diagram. Phase diagrams for the other five combinations of CaM and r_1 are shown in Fig. S16. The phase plot reveals an interesting and unexpected feature of this model; at high calcium concentrations and low to intermediate PP1 concentrations, increases in

PP1 increase the total kinase activity of the system. It is generally assumed that increasing PP1 will reduce activity, because it will reduce the concentration of the autonomous state. Our model tracks the concentration of each CaMKII state, and we can therefore examine these curves to investigate the source of this surprising feature.

In Fig. 5, we plot the concentration of all six subunit states along with the concentration of active subunits as a function of PP1 at a fixed, high calcium concentration of $19.8 \mu\text{M}$. At low PP1, the dominant species is D_{up} , the doubly inactive state that must be dephosphorylated before it can be activated by CaM. Increasing PP1 converts more subunits to the unphosphorylated autoinhibited state, which can be directly activated by CaM. Thus, in this regime, PP1 aids in CaMKII activation by increasing the concentration of subunits available for CaM activation. Physiological PP1 concentrations are estimated to be in the 0.1 - to 1.0 - μM range, and therefore, this effect might be important in vivo. The demonstration of such an effect would be missed by less detailed models.

In the Supporting Material, we present results for a model with cooperative CaM binding to CaMKII, a mechanism suggested by some recent experimental results (82). There we show that the effects of cooperativity are negligible in the sense that cooperative CaM binding does not allow for any new qualitative behavior and does not shift activation thresholds or bistable regions down to basal calcium levels. This result is not surprising because the main model already contains strong cooperativity in calcium binding to

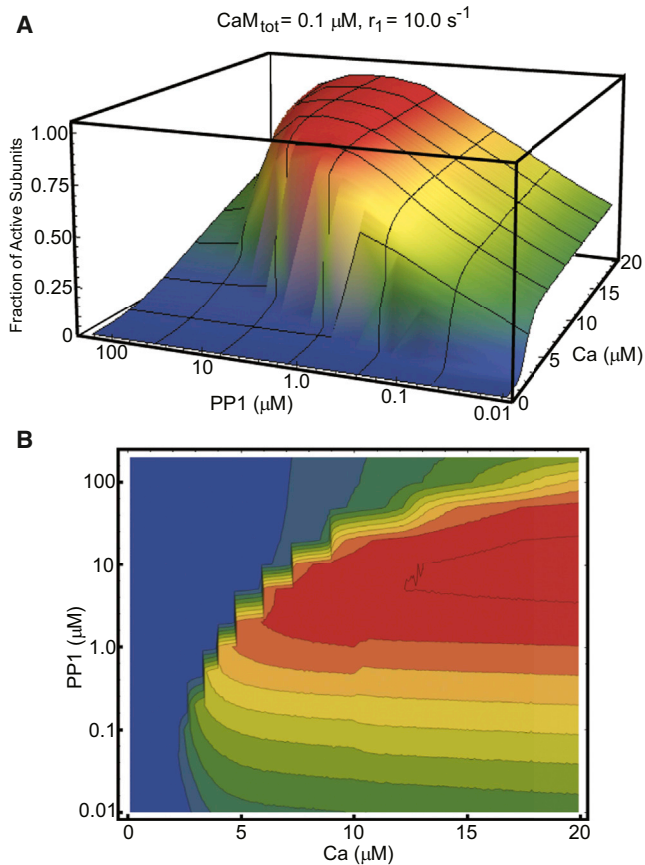


FIGURE 4 CaMKII activation phase diagram. (A) The curves shown in Fig. 3 are assembled into a single phase diagram showing CaMKII activity as a function of Ca^{2+} and PP1. (B) The phase diagram is shown as a contour plot.

CaM and in autophosphorylation of T286, so that a third additional source of cooperativity is unlikely to significantly alter the activation curves. See the [Supporting Material](#) for more details.

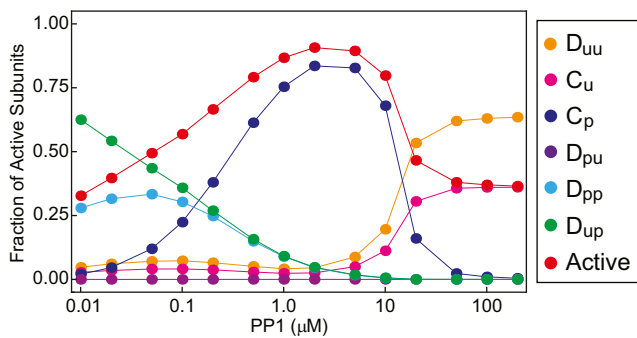


FIGURE 5 Detailed subunit distribution. The fraction of subunits in each state is plotted as a function of PP1 at high Ca^{2+} concentration, along with the fraction of active subunits. At low PP1, the dominant species are the doubly inhibited D_{up} and the autonomously active D_{pp} . At intermediate PP1, most subunits are CaM-bound and phosphorylated at T286. At very high PP1, all phosphorylation is suppressed and all subunits are either in the autoinhibited D_{uu} or the activated C_u state.

Dynamic behavior and response to stimuli

In this section, we examine the dynamic response of the system using typical *in vivo* concentrations and system parameters: $\text{CaMKII}_{\text{tot}} = 200 \mu\text{M}$, $\text{CaM}_{\text{tot}} = 5 \mu\text{M}$, $r_1 = 1 \text{ s}^{-1}$, and other parameters as listed in [Tables S1](#) and [S2](#). The CaM concentration used here is lower than that typically measured *in vivo*, but we use this lower value because our model does not include other CaM-binding proteins that significantly reduce the amount of CaM available for CaMKII activation. We varied I1 and PP1 to cover a range of *in vivo* estimates: 0, 0.01, and 0.1 μM I1_{tot}; 0.05, 0.1, 0.2, 0.5, and 1.0 μM PP1_{tot}. We used two different stimulation protocols, an LTP protocol consisting of high-amplitude, high-frequency stimulation (10 μM , 5 ms Ca^{2+} pulses at 100 Hz for 1 s), and an LTD protocol consisting of lower-amplitude, low-frequency stimulation (2 μM , 200 ms Ca^{2+} pulses at 1 Hz for 10 min). As discussed in the Model section, our assumptions of rapid equilibrium between Ca^{2+} and CaM break down on these fast timescales, as does the assumption that only fully saturated CaM can activate CaMKII. The activation curves shown here therefore overestimate the amount of CaMKII activation, but the qualitative features will be the same. Moreover, as shown below, the timescales of deactivation are slow enough for our model assumptions to be valid, and we can therefore make both qualitative and quantitative statements about the kinetics of deactivation.

Typically, stimulation protocols are modeled with initial conditions such that all CaMKII is in the autoinhibited state, D_{uu} (51). We hypothesized that applying these protocols to a system already in steady state would produce a significantly attenuated response because of the large concentration of doubly inhibited subunits. Thus, for all simulations, we applied the stimulation protocol twice: all simulations begin with 100% D_{uu} , and the stimulation protocol is applied. After the stimulation protocol, calcium is returned to basal levels and the system is allowed to relax to its basal steady state. Once steady state is achieved, the stimulation protocol is applied a second time and the time evolution of the system is followed until the system again relaxes back to its basal steady state.

Fig. 6 shows illustrative examples of the CaMKII activity produced by these protocols. In Fig. 6 A, the LTD protocol is applied to the system with 0.1 μM I1_{tot} and 1.0 μM PP1_{tot}. This generates low levels of CaMKII activity, and the activity of CaMKII simply oscillates at the same frequency of the stimulation. The response to the second stimulation is nearly identical to the response to the first stimulation, because steady-state PP1 activity is high enough to keep only a negligible fraction of subunits in the doubly inhibited state. In Fig. 6 B, the LTD protocol is applied to a system with 0 μM I1_{tot} and 0.05 μM PP1_{tot}. Here, CaMKII activity slowly but steadily increases with each pulse, and the activity does not plateau

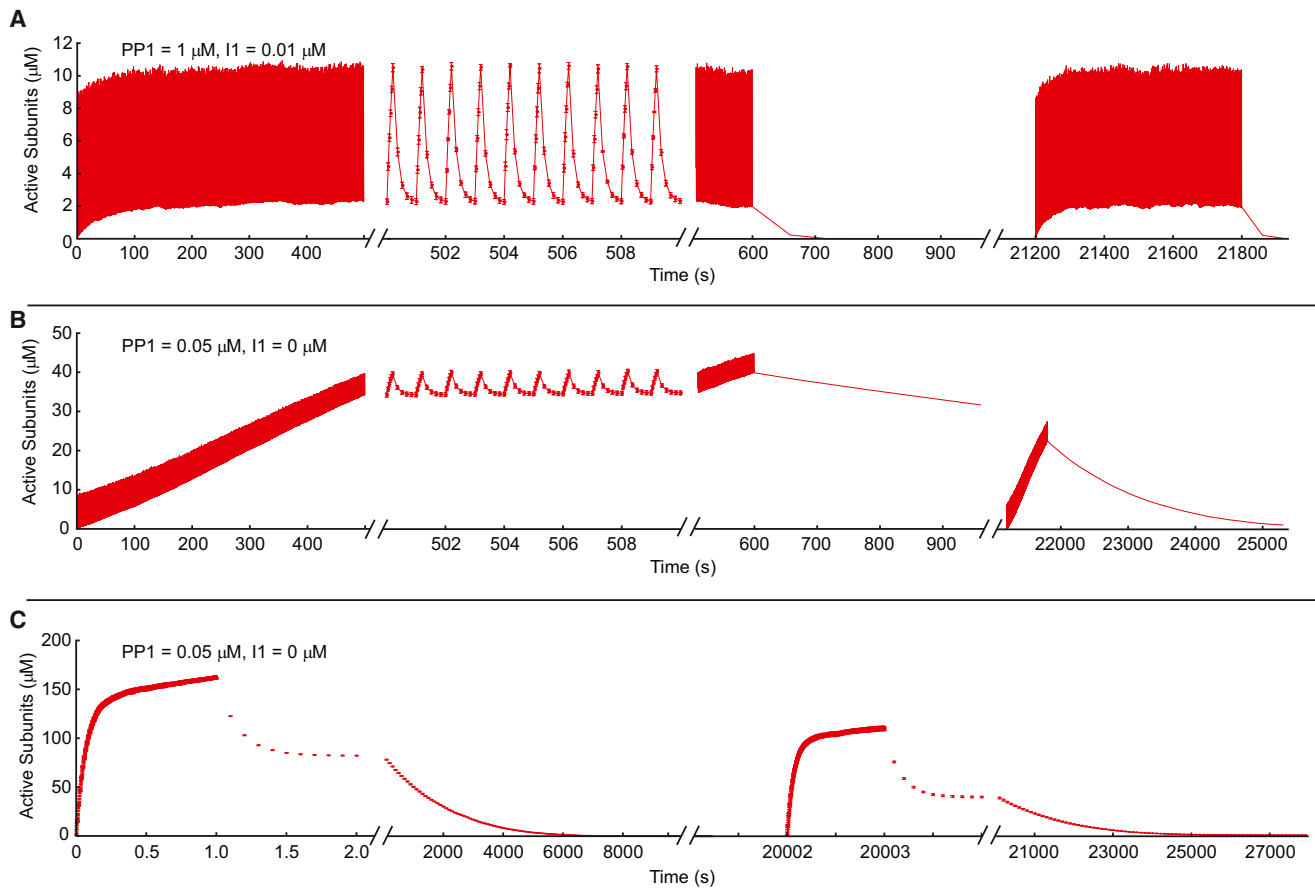


FIGURE 6 Response to LTP and LTD protocols. In each figure, the system begins with all subunits in the D_{aut} state, and the first stimulation protocol is applied at $t = 0$. After the first stimulation protocol, the system is allowed to relax to its steady state at basal calcium. We then apply a second stimulation protocol (identical to the first), after which the system is again allowed to relax to steady state. The axes are cut to highlight various sections of interest. (A) LTD protocol. In this case, CaMKII activity oscillates in time with the stimulation and there is no significant accumulation of active subunits. The first and second stimuli produce identical responses. (B) LTD protocol. In this case, CaMKII activity slowly accumulates with each pulse, and does not plateau during the time course of the stimulation. The response to the second stimulus is significantly attenuated, because a significant fraction of subunits are doubly inhibited in the steady state. (C) LTP protocol. CaMKII is rapidly activated and then plateaus. Activity decays in a biexponential manner with a very fast and a very slow time constant, as discussed in the text. The response to the second stimulus is attenuated, as in B. See the text for more details.

during the stimulation protocol. This system has lower PP1 activity, and here it is easy to see the effect of T305 phosphorylation on the second stimulation. CaMKII activity increases at a much slower rate, because dephosphorylation must occur before CaMKII activation, and this greatly reduces the total amount of activation. In Fig. 6 C, the LTP protocol is applied to the same system in Fig. 6 B, and this shows a typical response to the LTP protocol. CaMKII activity rapidly increases and then begins to plateau. As in Fig. 6 B, inhibitory T305 phosphorylation significantly reduces the amount of activity generated in response to the second stimulation.

It is obvious from Fig. 6 C that CaMKII activity decays with two timescales: the first represents calmodulin rapidly dissociating from CaMKII after the stimuli, whereas the second represents the slow decrease in autonomous activity due to the action of PP1. To characterize this decay we fit it to a double exponential,

$$\text{Activity}(t) = a_1 e^{-(t-t^*)/\tau_1} + a_2 e^{-(t-t^*)/\tau_2}, \quad (6)$$

where t^* is the time the last calcium pulse finishes and τ_1 and τ_2 characterize the fast and slow decay times, respectively. By requiring that $\tau_2 > \tau_1$, we can interpret $(a_1 + a_2)$ as the total CaMKII activity generated by the stimulation, and a_2 as the total autonomy generated by the stimulation.

We used this fit to characterize the result of the LTP stimulation as the concentrations of PP1 and I1 were varied. In Fig. 7, we show the dependence of the fitted parameters as a function of PP1 for $I1 = 0.01 \mu\text{M}$. Additional examples are shown in Fig. S17. Several trends are evident. First, a_1 , τ_1 , and a_2 are independent of PP1 for the first pulse. This makes sense, as all of the simulations begin with the same initial conditions and the first pulse occurs on a time-scale too short to be affected by PP1. Second, the time constant for the decay of autonomous activity is a highly

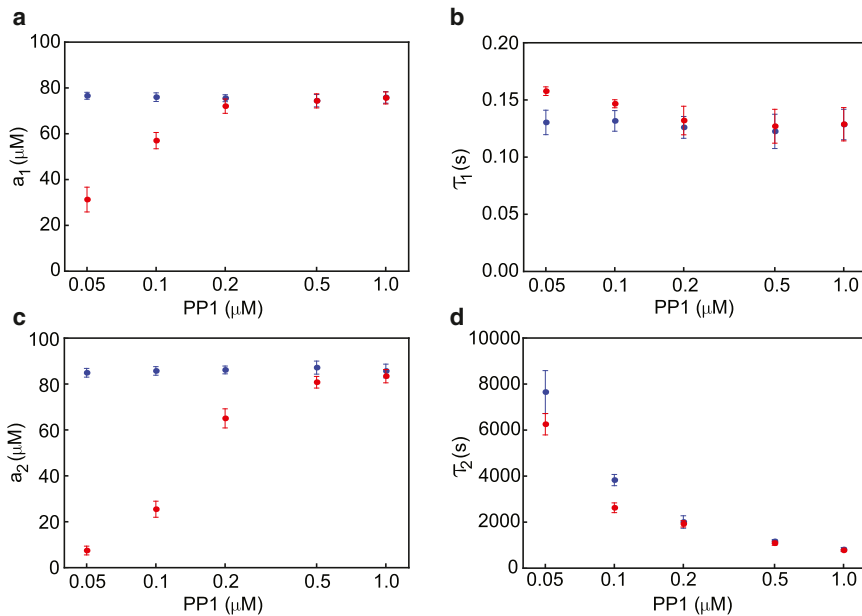


FIGURE 7 Characterization of response to LTP protocols. The decay of CaMKII activity after LTP stimulation was fit to a double exponential, and the fitted parameters are plotted as functions of PP1. The response to the first stimulation is shown in blue and the response to the second stimulation in red. (a) a_1 gives the concentration of active subunits that are CaM-bound but not phosphorylated, i.e., the nonautonomous portion of CaMKII activity. (b) τ_1 is the fast decay time, which is controlled by the dissociation of CaM from nonautonomous subunits. (c) a_2 gives the concentration of autonomous CaMKII generated in response to the stimulation protocol. (d) τ_2 characterizes the slow decay time for the loss of autonomous activity due to dephosphorylation.

nonlinear function of PP1, increasing dramatically as PP1 decreases. At $0.05 \mu\text{M}$ PP1, autonomous activity decays with a time constant of ~ 2 h.

For the second pulse (applied after steady state is reached), both the total activity and the amount of autonomous activity are significantly reduced at low PP1 concentrations. This reflects the fact that a significant fraction of the subunits are in the doubly inhibited D_{up} state at low PP1, and must be dephosphorylated before they can be activated by CaM. The fast and slow time constants are no different than during the first pulse, which is expected because τ_1 characterizes the dissociation of CaM and is not affected by phosphorylation, whereas τ_2 characterizes total PP1 activity, which is also unaffected by the initial phosphorylation state of the holoenzymes.

The simulations discussed above considered synaptic activation in the absence of background noise, and it is worthwhile to investigate the effects of noise on the system dynamics. In vivo, the largest source of noise is likely to be transient calcium fluctuations due to basal synaptic firing rates, which occur at ~ 1 Hz. A single synaptic activation produces postsynaptic calcium transients in the range 0.3 – $1.3 \mu\text{M}$ (95–97), although the duration of such transients in the spine is only 10 – 20 ms (97). We have repeated the LTP protocol in the presence of noise with a range of amplitudes and frequencies (0.1 – 2 Hz), and found that its effects were minimal. At the largest amplitudes and frequencies, spontaneous calcium transients could increase the deactivation time constant by about 10 – 20% , which is insignificant given uncertainties in other parameters, and in most cases spontaneous calcium transients produced no noticeable changes.

DISCUSSION

We have investigated the dynamic and steady-state properties of a detailed model of CaMKII by using a network-free simulation scheme, which allowed us to study the system without making the severe approximations that have characterized previous modeling efforts. We were particularly interested to determine whether bistability, a major feature of coarse-grained models, would still be present in a more detailed simulation. We found that our model produces regions of bistability, but for any reasonable choice of parameters bistability only occurs at calcium concentrations much higher than basal calcium levels, and then only over a relatively narrow calcium range. Because bistability does not occur at basal calcium levels, our model suggests that bistability is not a physiologically relevant feature of the CaMKII system, and therefore, despite its theoretical appeal, the CaMKII-PP1 system does not function as the bistable biochemical switch underlying synaptic plasticity and memory.

We reached this conclusion after sampling the parameter space over both physiological and extreme cases. Nevertheless, the full parameter space is too large to sample entirely, and it is possible that parameters could be found that would give broad regions of bistability at basal calcium levels. Furthermore, although we have included CaMKII phosphorylation sites known to affect kinase activity and/or CaM binding, there are several other phosphorylation sites whose functional role is unknown. It is possible that other CaMKII states would change the conclusions of this study, and the model may need to be revised as more biochemical details become known. Ultimately, careful experimental investigations will be required to reach a definitive conclusion on the existence and/or role of CaMKII bistability.

Our model predicts that CaMKII activity is not a simple Hill-like function of calcium for any physiologically reasonable choice of parameters. Rather, for low PP1, CaMKII activity turns on in a laser transition, whereas for higher PP1, CaMKII activity turns on abruptly just past the narrow region of bistability. Both types of activation curves are characterized by a threshold calcium level below which there is almost no activity. A sharp activation threshold is therefore a robust feature of our model, and it is interesting to speculate on the advantage of this characteristic as opposed to the robust bistability that emerged from other models. In a bistable system, there is a threshold stimulation required to drive the system to its high-activity state, but thereafter, all information about the threshold is lost and the system is insensitive to the characteristics of additional stimuli. With laserlike or steplike activity curves, activation always requires an above-threshold stimulus. A bistable system has a built-in frequency dependence because repetitive subsaturating (but above threshold) stimuli can drive the system to a high-activity state, provided the activating stimuli are fast enough to prevent the system from fully relaxing to the low-activity state between stimuli. The laserlike and steplike activation curves possess the same type of frequency dependence but are able to discriminate between a larger range of frequencies, because they are not automatically driven to a permanently active state once a critical activity level is attained. The frequency response at a specific synapse could be tuned by changing PP1 activity, which controls the decay rate to the low-activity state.

Our model included inhibitory autophosphorylation on T305, a feature that has been omitted in previous studies of bistability (but has been included in some models investigating very-short-time in vitro dynamics (84)). We found that this phosphorylation site dramatically changes the steady-state activity levels of CaMKII. In particular, at low-to-intermediate PP1 concentrations, the effect of T305 phosphorylation is to make CaMKII activity an increasing function of PP1 concentration. This was a surprising discovery, because PP1 deactivates autonomous activity, and is thus usually associated with reduced CaMKII activity. However, at low PP1, a significant fraction of subunits are phosphorylated on T305 in the steady state, and these subunits must be dephosphorylated before they can undergo CaM-mediated activation. Increasing PP1 therefore increases the fraction of subunits available for CaM binding, and increases the overall activity level of the system. It is only at very high PP1 that increasing PP1 decreases total activity.

It is conventional to characterize the system response to different LTP protocols under different conditions by the probability of switching to the highly active state (51). Such a characterization is impossible here, because our system does not exhibit bistability at basal calcium levels. In fact, the main differences between different stimulation protocols are in the rate at which CaMKII is activated and the maximum activity level attained. For example, there is no

fundamental difference between LTP and LTD protocols in this model; LTD protocols are simply characterized by a slower increase in CaMKII activity and a lower overall activity level compared to LTP protocols. As with the steady-state activity, we find that inhibitory phosphorylation at T305 has a significant effect on the dynamic response of the system. The total activity level achieved during a stimulation protocol is significantly reduced if the system begins in the basal steady state instead of with all subunits in the nonphosphorylated autoinhibited state. It takes time for the stimulation to dephosphorylate doubly inhibited subunits to make those subunits available for CaM binding, and this delay is sufficient to reduce the total activity achieved.

Basal inhibitory autophosphorylation on T305 is usually omitted in models, because the basal phosphorylation rate is extremely slow, $r_b = 5 \times 10^{-4} \text{ s}^{-1}$ in vitro (74). Thus, it is questionable whether the effects discussed above are relevant in vivo, where basal phosphatase activity might be sufficient to keep inhibitory autophosphorylation at negligible levels. However, the total fraction of phospho-T305 at resting levels is much higher than would be predicted by the slow measured in vitro phosphorylation rate (98), which suggests that basal autophosphorylation is accelerated by some undetermined mechanism. One potential mechanism is binding to the scaffold protein CASK, which has been shown to increase T305 phosphorylation 40-fold (75).

A significant feature of our model is the extremely slow PP1-mediated deactivation reaction. The decay from a highly active transient state to the resting level at basal calcium can take hours to days under relevant in vivo conditions. Most experiments that investigate in vivo bistability only track CaMKII activity for about an hour after stimulation protocols (37), and the longest experiment we are aware of only followed CaMKII activity for 8 h after stimulation (33). Our model suggests that a transiently active state could maintain autonomy over such timescales and may be interpreted as permanently elevated CaMKII activity. This observation suggests that the conflicting reports of CaMKII bistability may reflect the fact that transient activity could last for the duration of the experiment under typical conditions.

During LTP induction, CaMKII translocates to the PSD (99,100) by binding to NMDARs and other scaffold proteins (101,102). The CaMKII-NMDAR interaction is known to alter several important reaction rates (103), for example, decreasing the T286 dephosphorylation rate (104), and NMDAR-binding generates autonomous activity even without T286 phosphorylation (105). Our model does not include NMDAR binding, and we are therefore not able to investigate the effects of this important in vivo interaction. It is possible that NMDAR interactions could generate bistable kinase activity at basal calcium levels, but we feel that this is unlikely. The major effect of NMDAR binding

appears to be on the rate of dephosphorylation, which could have an effect on the qualitative aspects of the activation curve but would not shift the region of bistability to low calcium concentrations. Note that this only applies to bistability in CaMKII kinase activity. The CaMKII-NMDAR interaction is required for LTP maintenance (106), which suggests that CaMKII may play a structural role in synaptic plasticity.

In conclusion, our detailed model strongly suggests that CaMKII kinase activity is not the bistable molecular correlate to long-term memory. It also shows that the often overlooked inhibitory autophosphorylation on T305 can alter the system response to PP1 in such a way that PP1 actually increases CaMKII activity. Finally, the model suggests that previous observations of *in vivo* bistability were in fact observations of extremely long-lived transient states of high activity.

SUPPORTING MATERIAL

Two tables, 20 figures, references (107,108), and a supporting description of the model are available at [http://www.biophysj.org/biophysj/supplemental/S0006-3495\(13\)00747-9](http://www.biophysj.org/biophysj/supplemental/S0006-3495(13)00747-9).

I thank Leslie Loew for many helpful discussions and suggestions regarding both this work and the manuscript.

This work was supported by National Institutes of Health postdoctoral fellowship 1F32 NS077751-01 and grant P41 RR013186.

REFERENCES

- Brown, T. H., E. W. Kairiss, and C. L. Keenan. 1990. Hebbian synapses: biophysical mechanisms and algorithms. *Annu. Rev. Neurosci.* 13:475–511.
- Lamprecht, R., and J. LeDoux. 2004. Structural plasticity and memory. *Nat. Rev. Neurosci.* 5:45–54.
- Holtmaat, A., and K. Svoboda. 2009. Experience-dependent structural synaptic plasticity in the mammalian brain. *Nat. Rev. Neurosci.* 10:647–658.
- Caroni, P., F. Donato, and D. Müller. 2012. Structural plasticity upon learning: regulation and functions. *Nat. Rev. Neurosci.* 13:478–490.
- Malenka, R. C., and R. A. Nicoll. 1999. Long-term potentiation—a decade of progress? *Science.* 285:1870–1874.
- Malenka, R. C., and M. F. Bear. 2004. LTP and LTD: an embarrassment of riches. *Neuron.* 44:5–21.
- Kasai, H., M. Matsuzaki, ..., H. Nakahara. 2003. Structure-stability-function relationships of dendritic spines. *Trends Neurosci.* 26: 360–368.
- Sheng, M., and M. J. Kim. 2002. Postsynaptic signaling and plasticity mechanisms. *Science.* 298:776–780.
- Kennedy, M. B., H. C. Beale, ..., L. R. Washburn. 2005. Integration of biochemical signalling in spines. *Nat. Rev. Neurosci.* 6:423–434.
- Kelleher, 3rd, R. J., A. Govindarajan, and S. Tonegawa. 2004. Translational regulatory mechanisms in persistent forms of synaptic plasticity. *Neuron.* 44:59–73.
- Murakoshi, H., and R. Yasuda. 2012. Postsynaptic signaling during plasticity of dendritic spines. *Trends Neurosci.* 35:135–143.
- Crick, F. 1984. Memory and molecular turnover. *Nature.* 312:101.
- Lisman, J. E. 1985. A mechanism for memory storage insensitive to molecular turnover: a bistable autophosphorylating kinase. *Proc. Natl. Acad. Sci. USA.* 82:3055–3057.
- Kuret, J., and H. Schulman. 1985. Mechanism of autophosphorylation of the multifunctional Ca²⁺/calmodulin-dependent protein kinase. *J. Biol. Chem.* 260:6427–6433.
- Miller, S. G., and M. B. Kennedy. 1986. Regulation of brain type II Ca²⁺/calmodulin-dependent protein kinase by autophosphorylation: a Ca²⁺-triggered molecular switch. *Cell.* 44:861–870.
- Erondu, N. E., and M. B. Kennedy. 1985. Regional distribution of type II Ca²⁺/calmodulin-dependent protein kinase in rat brain. *J. Neurosci.* 5:3270–3277.
- Wayman, G. A., Y.-S. Lee, ..., T. R. Soderling. 2008. Calmodulin-kinases: modulators of neuronal development and plasticity. *Neuron.* 59:914–931.
- Lou, L. L., and H. Schulman. 1989. Distinct autophosphorylation sites sequentially produce autonomy and inhibition of the multifunctional Ca²⁺/calmodulin-dependent protein kinase. *J. Neurosci.* 9:2020–2032.
- Hashimoto, Y., C. M. Schworer, ..., T. R. Soderling. 1987. Autophosphorylation of Ca²⁺/calmodulin-dependent protein kinase II. Effects on total and Ca²⁺-independent activities and kinetic parameters. *J. Biol. Chem.* 262:8051–8055.
- Strack, S., M. A. Barban, ..., R. J. Colbran. 1997. Differential inactivation of postsynaptic density-associated and soluble Ca²⁺/calmodulin-dependent protein kinase II by protein phosphatases 1 and 2A. *J. Neurochem.* 68:2119–2128.
- Lisman, J., H. Schulman, and H. Cline. 2002. The molecular basis of CaMKII function in synaptic and behavioural memory. *Nat. Rev. Neurosci.* 3:175–190.
- Malenka, R. C., J. A. Kauer, ..., M. N. Waxham. 1989. An essential role for postsynaptic calmodulin and protein kinase activity in long-term potentiation. *Nature.* 340:554–557.
- Malinow, R., H. Schulman, and R. W. Tsien. 1989. Inhibition of postsynaptic PKC or CaMKII blocks induction but not expression of LTP. *Science.* 245:862–866.
- Pettit, D. L., S. Perlman, and R. Malinow. 1994. Potentiated transmission and prevention of further LTP by increased CaMKII activity in postsynaptic hippocampal slice neurons. *Science.* 266:1881–1885.
- Lledo, P.-M., G. O. Hjelmstad, ..., R. A. Nicoll. 1995. Calcium/calmodulin-dependent kinase II and long-term potentiation enhance synaptic transmission by the same mechanism. *Proc. Natl. Acad. Sci. USA.* 92:11175–11179.
- Silva, A. J., C. F. Stevens, ..., Y. Wang. 1992. Deficient hippocampal long-term potentiation in α -calcium-calmodulin kinase II mutant mice. *Science.* 257:201–206.
- Silva, A. J., R. Paylor, ..., S. Tonegawa. 1992. Impaired spatial learning in α -calcium-calmodulin kinase II mutant mice. *Science.* 257:206–211.
- Frankland, P. W., C. O'Brien, ..., A. J. Silva. 2001. α -CaMKII-dependent plasticity in the cortex is required for permanent memory. *Nature.* 411:309–313.
- Mayford, M., M. E. Bach, ..., E. R. Kandel. 1996. Control of memory formation through regulated expression of a CaMKII transgene. *Science.* 274:1678–1683.
- Patton, B. L., S. S. Molloy, and M. B. Kennedy. 1993. Autophosphorylation of type II CaM kinase in hippocampal neurons: localization of phospho- and dephosphokinase with complementary phosphorylation site-specific antibodies. *Mol. Biol. Cell.* 4:159–172.
- Ouyang, Y., D. Kantor, ..., M. B. Kennedy. 1997. Visualization of the distribution of autophosphorylated calcium/calmodulin-dependent protein kinase II after tetanic stimulation in the CA1 area of the hippocampus. *J. Neurosci.* 17:5416–5427.
- Makhinson, M., J. K. Chotiner, ..., T. J. O'Dell. 1999. Adenylyl cyclase activation modulates activity-dependent changes in synaptic

- strength and Ca^{2+} /calmodulin-dependent kinase II autophosphorylation. *J. Neurosci.* 19:2500–2510.
33. Ahmed, T., and J. U. Frey. 2005. Plasticity-specific phosphorylation of CaMKII, MAP-kinases and CREB during late-LTP in rat hippocampal slices in vitro. *Neuropharmacology.* 49:477–492.
 34. Lee, S.-J. R., Y. Escobedo-Lozoya, ..., R. Yasuda. 2009. Activation of CaMKII in single dendritic spines during long-term potentiation. *Nature.* 458:299–304.
 35. Buard, I., S. J. Coultrap, ..., K. U. Bayer. 2010. CaMKII “autonomy” is required for initiating but not for maintaining neuronal long-term information storage. *J. Neurosci.* 30:8214–8220.
 36. Giese, K. P., N. B. Fedorov, ..., A. J. Silva. 1998. Autophosphorylation at Thr²⁸⁶ of the α calcium-calmodulin kinase II in LTP and learning. *Science.* 279:870–873.
 37. Fukunaga, K., L. Stoppini, ..., D. Muller. 1993. Long-term potentiation is associated with an increased activity of Ca^{2+} /calmodulin-dependent protein kinase II. *J. Biol. Chem.* 268:7863–7867.
 38. Fukunaga, K., D. Muller, and E. Miyamoto. 1995. Increased phosphorylation of Ca^{2+} /calmodulin-dependent protein kinase II and its endogenous substrates in the induction of long-term potentiation. *J. Biol. Chem.* 270:6119–6124.
 39. Feng, T. P. 1995. The involvement of PKC and multifunctional CaM kinase II of the postsynaptic neuron in induction and maintenance of long-term potentiation. *Prog. Brain Res.* 105:55–63.
 40. Wang, J. H., and P. T. Kelly. 1996. The balance between postsynaptic Ca^{2+} -dependent protein kinase and phosphatase activities controlling synaptic strength. *Learn. Mem.* 3:170–181.
 41. Lengyel, I., K. Voss, ..., T. V. P. Bliss. 2004. Autonomous activity of CaMKII is only transiently increased following the induction of long-term potentiation in the rat hippocampus. *Eur. J. Neurosci.* 20:3063–3072.
 42. Hvalby, Ø., H. C. Hemmings, Jr., ..., P. Andersen. 1994. Specificity of protein kinase inhibitor peptides and induction of long-term potentiation. *Proc. Natl. Acad. Sci. USA.* 91:4761–4765.
 43. Otmakhov, N., L. C. Griffith, and J. E. Lisman. 1997. Postsynaptic inhibitors of calcium/calmodulin-dependent protein kinase type II block induction but not maintenance of pairing-induced long-term potentiation. *J. Neurosci.* 17:5357–5365.
 44. Chen, H.-X., N. Otmakhov, ..., J. E. Lisman. 2001. Is persistent activity of calmodulin/calmodulin-dependent kinase required for the maintenance of LTP? *J. Neurophysiol.* 85:1368–1376.
 45. Yang, H.-W., X.-D. Hu, ..., X.-G. Liu. 2004. Roles of CaMKII, PKA, and PKC in the induction and maintenance of LTP of C-fiber-evoked field potentials in rat spinal dorsal horn. *J. Neurophysiol.* 91:1122–1133.
 46. Bradshaw, J. M., Y. Kubota, ..., H. Schulman. 2003. An ultrasensitive Ca^{2+} /calmodulin-dependent protein kinase II-protein phosphatase 1 switch facilitates specificity in postsynaptic calcium signaling. *Proc. Natl. Acad. Sci. USA.* 100:10512–10517.
 47. Kotaleski, J. H., and K. T. Blackwell. 2010. Modelling the molecular mechanisms of synaptic plasticity using systems biology approaches. *Nat. Rev. Neurosci.* 11:239–251.
 48. Manninen, T., K. Hituri, ..., M.-L. Linne. 2010. Postsynaptic signal transduction models for long-term potentiation and depression. *Front. Comput. Neurosci.* 4:152.
 49. Lisman, J. E., and M. A. Goldring. 1988. Feasibility of long-term storage of graded information by the Ca^{2+} /calmodulin-dependent protein kinase molecules of the postsynaptic density. *Proc. Natl. Acad. Sci. USA.* 85:5320–5324.
 50. Lisman, J. E. 1989. A mechanism for the Hebb and the anti-Hebb processes underlying learning and memory. *Proc. Natl. Acad. Sci. USA.* 86:9574–9578.
 51. Zhabotinsky, A. M. 2000. Bistability in the Ca^{2+} /calmodulin-dependent protein kinase-phosphatase system. *Biophys. J.* 79:2211–2221.
 52. Graupner, M., and N. Brunel. 2007. STDP in a bistable synapse model based on CaMKII and associated signaling pathways. *PLOS Comput. Biol.* 3:e221.
 53. Miller, P., A. M. Zhabotinsky, ..., X.-J. Wang. 2005. The stability of a stochastic CaMKII switch: dependence on the number of enzyme molecules and protein turnover. *PLoS Biol.* 3:e107.
 54. Michalski, P. J., and L. M. Loew. 2012. CaMKII activation and dynamics are independent of the holoenzyme structure: an infinite subunit holoenzyme approximation. *Phys. Biol.* 9:036010.
 55. Xia, Z., and D. R. Storm. 2005. The role of calmodulin as a signal integrator for synaptic plasticity. *Nat. Rev. Neurosci.* 6:267–276.
 56. Crouch, T. H., and C. B. Klee. 1980. Positive cooperative binding of calcium to bovine brain calmodulin. *Biochemistry.* 19:3692–3698.
 57. Linse, S., A. Helmersson, and S. Forsén. 1991. Calcium binding to calmodulin and its globular domains. *J. Biol. Chem.* 266:8050–8054.
 58. Peersen, O. B., T. S. Madsen, and J. J. Falke. 1997. Intermolecular tuning of calmodulin by target peptides and proteins: differential effects on Ca^{2+} binding and implications for kinase activation. *Protein Sci.* 6:794–807.
 59. Byrne, M. J., J. A. Putkey, ..., Y. Kubota. 2009. Dissecting cooperative calmodulin binding to CaM kinase II: a detailed stochastic model. *J. Comput. Neurosci.* 27:621–638.
 60. Pepke, S., T. Kinzer-Ursem, ..., M. B. Kennedy. 2010. A dynamic model of interactions of Ca^{2+} , calmodulin, and catalytic subunits of Ca^{2+} /calmodulin-dependent protein kinase II. *PLOS Comput. Biol.* 6:e1000675.
 61. Chiba, H., N. S. Schneider, ..., A. Noma. 2008. A simulation study on the activation of cardiac CaMKII δ -isoform and its regulation by phosphatases. *Biophys. J.* 95:2139–2149.
 62. Faas, G. C., S. Raghavachari, ..., I. Mody. 2011. Calmodulin as a direct detector of Ca^{2+} signals. *Nat. Neurosci.* 14:301–304.
 63. Chao, L. H., M. M. Stratton, ..., J. Kuriyan. 2011. A mechanism for tunable autoinhibition in the structure of a human Ca^{2+} /calmodulin-dependent kinase II holoenzyme. *Cell.* 146:732–745.
 64. Kolodziej, S. J., A. Hudmon, ..., J. K. Stoops. 2000. Three-dimensional reconstructions of calcium/calmodulin-dependent (CaM) kinase II α and truncated CaM kinase II α reveal a unique organization for its structural core and functional domains. *J. Biol. Chem.* 275:14354–14359.
 65. Morris, E. P., and K. Török. 2001. Oligomeric structure of α -calmodulin-dependent protein kinase II. *J. Mol. Biol.* 308:1–8.
 66. Gaertner, T. R., S. J. Kolodziej, ..., M. N. Waxham. 2004. Comparative analyses of the three-dimensional structures and enzymatic properties of α , β , γ and δ isoforms of Ca^{2+} -calmodulin-dependent protein kinase II. *J. Biol. Chem.* 279:12484–12494.
 67. Rellos, P., A. C. W. Pike, ..., S. Knapp. 2010. Structure of the CaMKII δ /calmodulin complex reveals the molecular mechanism of CaMKII kinase activation. *PLoS Biol.* 8:e1000426.
 68. Hanson, P. I., T. Meyer, ..., H. Schulman. 1994. Dual role of calmodulin in autophosphorylation of multifunctional CaM kinase may underlie decoding of calcium signals. *Neuron.* 12:943–956.
 69. Mukherji, S., and T. R. Soderling. 1994. Regulation of Ca^{2+} /calmodulin-dependent protein kinase II by inter- and intrasubunit-catalyzed autophosphorylations. *J. Biol. Chem.* 269:13744–13747.
 70. Rich, R. C., and H. Schulman. 1998. Substrate-directed function of calmodulin in autophosphorylation of Ca^{2+} /calmodulin-dependent protein kinase II. *J. Biol. Chem.* 273:28424–28429.
 71. Coultrap, S. J., I. Buard, ..., K. U. Bayer. 2010. CaMKII autonomy is substrate-dependent and further stimulated by Ca^{2+} /calmodulin. *J. Biol. Chem.* 285:17930–17937.
 72. Hanson, P. I., and H. Schulman. 1992. Inhibitory autophosphorylation of multifunctional Ca^{2+} /calmodulin-dependent protein kinase analyzed by site-directed mutagenesis. *J. Biol. Chem.* 267:17216–17224.

73. Lengyel, I., S. Fieuw-Makaroff, ..., P. R. Dunkley. 2000. Modulation of the phosphorylation and activity of calcium/calmodulin-dependent protein kinase II by zinc. *J. Neurochem.* 75:594–605.
74. Colbran, R. J. 1993. Inactivation of Ca²⁺/calmodulin-dependent protein kinase II by basal autophosphorylation. *J. Biol. Chem.* 268:7163–7170.
75. Lu, C. S., J. J. L. Hodge, ..., L. C. Griffith. 2003. Regulation of the Ca²⁺/CaM-responsive pool of CaMKII by scaffold-dependent autophosphorylation. *Neuron.* 40:1185–1197.
76. Shifman, J. M., M. H. Choi, ..., M. B. Kennedy. 2006. Ca²⁺/calmodulin-dependent protein kinase II (CaMKII) is activated by calmodulin with two bound calciums. *Proc. Natl. Acad. Sci. USA.* 103:13968–13973.
77. Forest, A., M. T. Swulius, ..., M. N. Waxham. 2008. Role of the N- and C-lobes of calmodulin in the activation of Ca²⁺/calmodulin-dependent protein kinase II. *Biochemistry.* 47:10587–10599.
78. Meyer, T., P. I. Hanson, ..., H. Schulman. 1992. Calmodulin trapping by calcium-calmodulin-dependent protein kinase. *Science.* 256:1199–1202.
79. Singla, S. I., A. Hudmon, ..., H. Schulman. 2001. Molecular characterization of calmodulin trapping by calcium/calmodulin-dependent protein kinase II. *J. Biol. Chem.* 276:29353–29360.
80. Rosenberg, O. S., S. Deindl, ..., J. Kuriyan. 2005. Structure of the autoinhibited kinase domain of CaMKII and SAXS analysis of the holoenzyme. *Cell.* 123:849–860.
81. Thaler, C., S. V. Koushik, ..., S. S. Vogel. 2009. Structural rearrangement of CaMKII α catalytic domains encodes activation. *Proc. Natl. Acad. Sci. USA.* 106:6369–6374.
82. Chao, L. H., P. Pellicena, ..., J. Kuriyan. 2010. Intersubunit capture of regulatory segments is a component of cooperative CaMKII activation. *Nat. Struct. Mol. Biol.* 17:264–272.
83. De Koninck, P., and H. Schulman. 1998. Sensitivity of CaM kinase II to the frequency of Ca²⁺ oscillations. *Science.* 279:227–230.
84. Lucić, V., G. J. Greif, and M. B. Kennedy. 2008. Detailed state model of CaMKII activation and autophosphorylation. *Eur. Biophys. J.* 38:83–98.
85. Coultrap, S. J., K. Barcomb, and K. U. Bayer. 2012. A significant but rather mild contribution of T286 autophosphorylation to Ca²⁺/CaM-stimulated CaMKII activity. *PLoS ONE.* 7:e37176.
86. Nairn, A. C., and S. Shenolikar. 1992. The role of protein phosphatases in synaptic transmission, plasticity and neuronal development. *Curr. Opin. Neurobiol.* 2:296–301.
87. Mulkey, R. M., S. Endo, ..., R. C. Malenka. 1994. Involvement of a calcineurin/inhibitor-1 phosphatase cascade in hippocampal long-term depression. *Nature.* 369:486–488.
88. Stemmer, P. M., and C. B. Klee. 1994. Dual calcium ion regulation of calcineurin by calmodulin and calcineurin B. *Biochemistry.* 33:6859–6866.
89. Smith, S. B., H. D. White, ..., E. G. Krebs. 1981. Cyclic AMP-dependent protein kinase I: cyclic nucleotide binding, structural changes, and release of the catalytic subunits. *Proc. Natl. Acad. Sci. USA.* 78:1591–1595.
90. Tang, W.-J., J. Krupinski, and A. G. Gilman. 1991. Expression and characterization of calmodulin-activated (type I) adenylyl cyclase. *J. Biol. Chem.* 266:8595–8603.
91. Tang, W.-J., and A. G. Gilman. 1992. Adenylyl cyclases. *Cell.* 70:869–872.
92. Beavo, J. A. 1995. Cyclic nucleotide phosphodiesterases: functional implications of multiple isoforms. *Physiol. Rev.* 75:725–748.
93. Sneddon, M. W., J. R. Faeder, and T. Emonet. 2011. Efficient modeling, simulation and coarse-graining of biological complexity with NFsim. *Nat. Methods.* 8:177–183.
94. Gillespie, D. T. 2007. Stochastic simulation of chemical kinetics. *Annu. Rev. Phys. Chem.* 58:35–55.
95. Müller, W., and J. A. Connor. 1991. Dendritic spines as individual neuronal compartments for synaptic Ca²⁺ responses. *Nature.* 354:73–76.
96. Murphy, T. H., J. M. Baraban, ..., L. A. Blatter. 1994. Visualization of quantal synaptic transmission by dendritic calcium imaging. *Science.* 263:529–532.
97. Sabatini, B. L., T. G. Oertner, and K. Svoboda. 2002. The life cycle of Ca²⁺ ions in dendritic spines. *Neuron.* 33:439–452.
98. Elgersma, Y., N. B. Fedorov, ..., A. J. Silva. 2002. Inhibitory autophosphorylation of CaMKII controls PSD association, plasticity, and learning. *Neuron.* 36:493–505.
99. Shen, K., and T. Meyer. 1999. Dynamic control of CaMKII translocation and localization in hippocampal neurons by NMDA receptor stimulation. *Science.* 284:162–166.
100. Shen, K., M. N. Teruel, ..., T. Meyer. 2000. Molecular memory by reversible translocation of calcium/calmodulin-dependent protein kinase II. *Nat. Neurosci.* 3:881–886.
101. Strack, S., and R. J. Colbran. 1998. Autophosphorylation-dependent targeting of calcium/calmodulin-dependent protein kinase II by the NR2B subunit of the N-methyl-D-aspartate receptor. *J. Biol. Chem.* 273:20689–20692.
102. Leonard, A. S., I. A. Lim, ..., J. W. Hell. 1999. Calcium/calmodulin-dependent protein kinase II is associated with the N-methyl-D-aspartate receptor. *Proc. Natl. Acad. Sci. USA.* 96:3239–3244.
103. Cheriyan, J., P. Kumar, ..., R. V. Omkumar. 2011. Calcium/calmodulin dependent protein kinase II bound to NMDA receptor 2B subunit exhibits increased ATP affinity and attenuated dephosphorylation. *PLoS ONE.* 6:e16495.
104. Mullasseril, P., A. Dosemeci, ..., L. C. Griffith. 2007. A structural mechanism for maintaining the “on-state” of the CaMKII memory switch in the post-synaptic density. *J. Neurochem.* 103:357–364.
105. Bayer, K. U., P. De Koninck, ..., H. Schulman. 2001. Interaction with the NMDA receptor locks CaMKII in an active conformation. *Nature.* 411:801–805.
106. Sanhueza, M., G. Fernandez-Villalobos, ..., J. Lisman. 2011. Role of the CaMKII/NMDA receptor complex in the maintenance of synaptic strength. *J. Neurosci.* 31:9170–9178.
107. Slepchenko, B. M., J. C. Schaff, ..., L. M. Loew. 2003. Quantitative cell biology with the Virtual Cell. *Trends Cell Biol.* 13:570–576.
108. Endo, S., X. Zhou, ..., S. Shenolikar. 1996. Multiple structural elements define the specificity of recombinant human inhibitor-1 as a protein phosphatase-1 inhibitor. *Biochemistry.* 35:5220–5228.

The Delicate Bistability of CaMKII

P. J. Michalski*

Richard D. Berlin Center for Cell Analysis and Modeling, University of Connecticut Health Center,
Farmington, Connecticut

Michalski

CaMKII Activation and Dynamics

Submitted February 27, 2013, and accepted for publication June 25, 2013.

*Correspondence: michalski@uchc.edu

Supporting Text

Modeling Platforms

We used a custom Java program to run network free simulations of the system described above. A nearly identical program was described in (1). Briefly, CaMKII holoenzymes are stored as $N \times 1$ arrays, where N is the number of subunits in a holoenzyme, where each array element stores the state of an individual subunit. Each subunit could undergo one of the three types of reactions described above, with actual transition probabilities determined by the current state of the subunit and the state of its neighboring subunits. For inter-subunit phosphorylation, the i th subunit could phosphorylate the $(i + 1)$ th subunit, and the N th subunit could phosphorylate the 1st subunit. All simulations contained a total of 6000 subunits ($6000/N$ holoenzymes), which 1) produced sufficiently small deviation from the mean without becoming too computationally taxing and 2) is approximately the number of subunits present in the PSD ($200 \mu\text{M}$ CaMKII in a PSD of radius $0.5 \mu\text{m}$ and height 50 nm). For steady state measurements, the system was run for a time T to reach steady state (T depends on the actual system parameters), then run for an additional time T while data was recorded (≥ 100 time points), and steady state values are reported as the averages and standard deviations of these time points. For time dependent measurements, data from at least 5 simulations were used to obtain averages and standard deviations at each time point. We have previously shown that the system properties become independent of holoenzyme size when there are six or more subunits per holoenzyme (1), and unless noted otherwise we used hexameric holoenzymes in all of the results shown below.

Particle-based stochastic simulations are generally much slower than deterministic numerical simulations. Some results reported here required extensive parameter searches (notably the comparison to experimental results), and for these searches we used either of two deterministic models based on a dimer holoenzyme, which requires few enough species to be practically implemented in conventional modeling software. For dynamic simulations we used a Virtual Cell (2) model described previously (1), while steady state solutions were explored using a custom Mathematica code. In all cases, once appropriate parameter ranges were identified, we used the particle-based Java simulation to obtain the results presented here.

Each model was verified by simulating sub-systems which could be compared to analytic results, and verified against each other for more general cases. The Java program and the Mathematica code are available upon request. The VCell model “CaMKII Dimer v2.0” is publicly available under the username `pjmichal`.

Model Validation

We validated the dynamic properties of the model by comparing the model results to the classic experiments of De Koninck and Schulman (3), which demonstrated the frequency dependence of CaMKII autonomy. In these experiments, CaMKII immobilized in a flow chamber was exposed to pulses of ATP and varying amounts of calcium-saturated CaM, and CaMKII autonomy was measured as a function of pulse duration and frequency. Figure S2 compares the model outputs to

the experimental results. Figure S2(A) shows the autonomy generated by a continuous 6 second pulse as the concentration of CaM is varied. Under the experimental conditions maximal autonomy is 80% of the maximal Ca^{2+} /CaM-stimulated activity. Thus, for our simulation results, we multiply the fraction of autonomous subunits by 0.8 to obtain a fractional autonomous activity. Figure S2(B) shows the autonomy generated by one hundred, 200 ms pulses as a function of time for stimuli of different frequencies. Autonomy is generated more rapidly by higher frequencies. Figure S2(C) shows autonomy is a highly non-linear function of frequency. For the experiments in Fig. S2(C), CaMKII was exposed to pulses of varying duration, but the total number of pulses was varied in order to keep the total stimulus exposure constant at 6 seconds. The system response depends on both the pulse duration and frequency. For all of these experiments, the model results are in excellent qualitative and quantitative agreement with the experimental results. We conclude that the model accurately captures CaMKII dynamics.

We validated the equilibrium properties of the model by comparing the model results against data from Ref. (4). These experiments measured steady state CaMKII autonomy as a function of Ca^{2+} as both total CaMKII and total PP1 were varied. No autonomous activity was detected at $0.2 \mu\text{M}$ CaMKII and $2.5 \mu\text{M}$ PP1, which suggests that autonomy was below the detection threshold in this assay. We included this detection threshold by plotting our simulation results as

$$\frac{A}{A_{\max}} = \frac{E - E_{\text{th}}}{E_{\max} - E_{\text{th}}} \quad \text{for } E > E_{\text{th}}, \quad (1)$$

where A is the measured autonomy, E is the concentration of active kinase subunits, and E_{th} is the threshold kinase concentration below which any activity is indistinguishable from background, and A is normalized to the maximum autonomy under the given conditions. We assume that E_{th} depends on the concentration of CaMKII but not on any other variables. This gave three free parameters, one each for Figs. S3(A), (B), and (C), which we found by a direct least-squares fit. The agreement between the model and the experimental data is excellent. Notably, the model does not predict any regions of bistability for these concentrations, in agreement with the experimental data.

Cooperative Calmodulin Binding

Early studies of CaMKII activation concluded that CaM binds CaMKII in a non-cooperative manner (see, for example, Fig. 2b in Ref. (3), or Fig. 2a in Ref. (4)), and this is the mechanism included in the model used in the main text. However, there is recent evidence that CaM binds CaMKII cooperatively (5), with measured Hill coefficients ranging from 1.5 to 4.3 depending on various mutations to the regulatory domain. It is not known why such cooperativity was missed in earlier studies. It has been proposed (6, 7) that cooperativity arises because the regulatory domains of neighboring subunits pair up in the autoinhibited holoenzyme; CaM binding to one subunit disrupts this interaction, making the previously paired regulatory domain readily available for CaM binding. The actual mechanism must be more complex because a simple dimerization mechanism cannot account for Hill coefficients larger than 2, and may involve the interaction of neighboring subunit dimers.

In order to assess whether the possibility of CaM cooperativity could affect our conclusion that bistability is an insignificant component of CaMKII physiology, we studied the effect of cooperative CaM binding using a dimer model for the CaMKII holoenzyme. Such a scheme will not reproduce the full extent of observed cooperativity, but will indicate how and to what extent activation curves will change as cooperativity is turned on. Cooperativity can be implemented by varying either the on or the off rates; here we choose to only vary the on rates. To determine how those rates should change, it is useful to consider CaM binding to CaMKII in the absence of phosphorylation reactions (which is realized in practice by making the mutations T286A/T305A/T306A). In this case each subunit is in one of two states, either inactive or CaM-bound, and the dimer can be in one of four possible configurations, denoted as M_{00} , M_{01} , M_{10} , and M_{11} , where the two indices refer to each subunit, and a 0 indicates an inactive subunit and a 1 indicates a CaM-bound subunit. The reaction scheme for this system is shown in Fig. S18, where CaM binding to the completely inhibited dimer occurs with an on-rate of βk_+ , and CaM binding to the partially active dimer occurs with an on-rate of αk_+ , and $\alpha = \beta = 1$ corresponds to the non-cooperative limit. The fraction of active subunits, A , is given by

$$A = \frac{M_{10} + M_{01} + M_{11}}{M_{\text{tot}}}, \quad (2)$$

where $M_{\text{tot}} = M_{00} + M_{10} + M_{01} + M_{11}$ is the total concentration of dimers. We can write this in terms of the total concentration of calcium-saturated CaM, C , as

$$A = \frac{2\alpha\beta \left(\frac{C}{K_0}\right) \left(\frac{1}{\alpha} + \frac{C}{K_0}\right)}{1 + 2\beta \left(\frac{C}{K_0}\right) + \alpha\beta \left(\frac{C}{K_0}\right)^2}, \quad (3)$$

where $K_0 = k_-/k_+$ is the non-cooperative dissociation constant. The effective dissociation constant, K_{eff} , is the CaM concentration giving 50% activity, and is given by

$$K_{\text{eff}} = \frac{K_0}{\sqrt{\alpha\beta}}. \quad (4)$$

In order to have a well-defined dissociation constant in the infinitely cooperatively limit, $\alpha \rightarrow \infty$, we must simultaneously take $\beta \rightarrow 0$, and we therefore set $\beta = 1/\alpha$.

In the full model, we assume that the dimerization of regulatory domains is disrupted by modifications which activate the kinase (either CaM-binding or T286 phosphorylation), but not by those which leave the kinase inactive (basal autophosphorylation on T305). Thus, if both subunits of a dimer are inactive, then the on-rate to both is reduced by a factor $1/\alpha$, while if either subunit is active, then the on-rate to both is increased by a factor α . The non-cooperative model is recovered by letting $\alpha = 1$. All other reactions remain as described in the main text. This scheme was implemented in a VCell model, “Dimer_CooperativeCaMBinding02”, which is publicly available under the username `pjmichal`. We ran and analyzed over 31000 simulations of this model in order to fully explore the relevant parameter space.

To begin, we verified that the dimer model recapitulates the activation curves of the hexamer discussed in the main text. We found that the dimer required a larger concentration of total

subunits in order to saturate the phosphatase and allow for any regions of bistability. We therefore increased the concentration of CaMKII subunits from 200 μM to 2000 μM . We used 100 μM CaM and the fast set of autophosphorylation rates, $r_1 = 10 \text{ s}^{-1}$. These conditions provided the lowest thresholds to activation (but still well above basal calcium levels) and give the best chance to observe cooperativity-induced changes which might alter the behavior at basal calcium levels. The non-cooperative activation curves for these conditions are shown in Fig. S19 and do indeed recapitulate the activation curves of the hexamer. As phosphatase activity increases, the activation curves go from laser-like to step-like (with narrow regions of bistability) and finally to Hill-like at very high phosphatase activity. Even at these high CaM concentrations and fast autophosphorylation rates, the regions of bistability occur at calcium concentration five times higher than basal levels.

When cooperativity is turned on we find no significant qualitative differences in the types of activation curves; that is, curves are always either laser-like, step-like (with narrow regions of bistability far above basal calcium), or Hill-like. However, for a given parameter set, cooperativity can convert one type of curve into another. We found five types of behavior:

- 1) Laser-like curve becomes Hill-like.
- 2) Step-like curve becomes laser-like.
- 3) Step-like curve remains step-like.
- 4) Hill-like curves becomes step-like.
- 5) Hill-like curve remains Hill-like but with a larger Hill coefficient.

These five behaviors are illustrated in Fig. S20, where we show how several curves from Fig. S19 evolve as α is increased in powers of 10 from 1 to 1000. (In each case we continued to increase α in powers of 10 up to 10^6 in order to verify a limiting behavior had been reached.) Importantly, even at these high CaM concentrations and fast autophosphorylation rates, the regions of bistability occur at calcium concentrations five times higher than basal levels. Additionally, as in the non-cooperative CaM case analyzed in the main text of this paper, the range of Ca^{2+} concentrations that display bistability are so small as to be physiologically negligible. We conclude that cooperative CaM binding does not change the qualitative behavior of CaMKII activation curves.

This conclusion is not surprising because there are already two mechanisms of cooperativity at work in CaMKII activation, namely, cooperative calcium binding to CaM and cooperative autophosphorylation on T286. These cooperative mechanism are sufficient to produce very large Hill coefficients and step-like activation curves, which are generally the main features associated with cooperative activation. Adding a third source of cooperativity to such a strongly cooperative system is unlikely to have a significant effect, as verified by the results above.

Supporting Tables

Parameter	Description	Value	Reference
K_0	Dissociation constant for Ca^{2+} binding CaM_0	$20 \mu\text{M}$	(8)
K_1	Dissociation constant for Ca^{2+} binding CaM_1	$0.57 \mu\text{M}$	(8)
K_2	Dissociation constant for Ca^{2+} binding CaM_2	$100 \mu\text{M}$	(8)
K_3	Dissociation constant for Ca^{2+} binding CaM_3	$5 \mu\text{M}$	(8)
$k_{\text{off},u}^{(1)}$	CaM_4 , D_{uu} direct dissociation rate	2 s^{-1}	(9, 10)
$k_{\text{off},u}^{(2)}$	CaM_4 , D_{uu} maximum Ca^{2+} -mediated dissociation rate	4.3 s^{-1}	Fit to data in Ref. (9)
$K_{\text{Ca},u}$	EC_{50} for CaM_4 , D_{uu} Ca^{2+} -mediated dissociation	$0.94 \mu\text{M}$	Fit to data in Ref. (9)
$k_{\text{on},u}$	CaM_4 , D_{uu} association rate	$30 \mu\text{M}^{-1} \text{ s}^{-1}$	Based on $k_{\text{off},u}$ and $K_D \approx 66.7 \text{ nM}$
$k_{\text{off},p}^{(1)}$	CaM_4 , D_{pu} direct dissociation rate	0.001 s^{-1}	(9)
$k_{\text{off},p}^{(2)}$	CaM_4 , D_{pu} maximum Ca^{2+} -mediated dissociation rate	0.08 s^{-1}	(9)
$K_{\text{Ca},p}$	EC_{50} for CaM_4 , D_{pu} Ca^{2+} -mediated dissociation	$0.19 \mu\text{M}$	(9)
$k_{\text{on},p}$	CaM_4 , D_{pu} association rate	$10 \mu\text{M}^{-1} \text{ s}^{-1}$	(9)
r_1	C_u -mediated T286 phosphorylation rate	1.0 s^{-1} or 10 s^{-1}	Order of magnitude estimate.
r_2	C_p -mediated T286 phosphorylation rate	r_1	Based on activity towards exogenous substrates.
r_3	D_{pu} -mediated T286 phosphorylation rate	$0.8r_1$	Based on autonomous activity towards exogenous substrates.
r_4	D_{pp} -mediated T286 phosphorylation rate	r_3	D_{pp} and D_{pu} have same activity towards exogenous substrates (11).
r_{305}	D_{pu} T305 autophosphorylation rate	10 s^{-1}	Order of magnitude estimate.
r_b	D_{uu} T305 basal autophosphorylation rate	$5 \times 10^{-4} \text{ s}^{-1}$	(12)

Table S1: Model parameters for Ca^{2+} -CaM binding and CaMKII autophosphorylation.

Parameter	Description	Value	Reference
k_{cat}	PP1-mediated CaMKII dephosphorylation rate.	1.72 s^{-1}	(4)
K_m	PP1-mediated CaMKII dephosphorylation Michaelis-Menton constant.	$11 \mu\text{M}$	(4)
$k_{\text{on,PP1}}$	I1, PP1 association rate	$500 \mu\text{M}^{-1} \text{ s}^{-1}$	(13)
$k_{\text{off,PP1}}$	I1, PP1 dissociation rate	0.1 s^{-1}	(13)
$k_{\text{CaN}}^{(0)}$	Basal CaN activity	0.1 s^{-1}	(14)
k_{CaN}	Maximum Ca/CaM stimulated CaN activity	18 s^{-1}	(14)
K_{CaN}	CaN activity EC_{50}	$0.053 \mu\text{M}$	(14)
n_{CaN}	CaN activity Hill coefficient	3	(14)
$k_{\text{PKA}}^{(0)}$	Basal PKA activity	0.0036 s^{-1}	(14)
k_{PKA}	Maximum Ca/CaM stimulated PKA activity	100 s^{-1}	(14)
K_{PKA}	PKA activity EC_{50}	$0.11 \mu\text{M}$	(14)
n_{PKA}	PKA activity Hill coefficient	8	(14)

Table S2: Model parameters for PP1 activity.

Supporting Figures

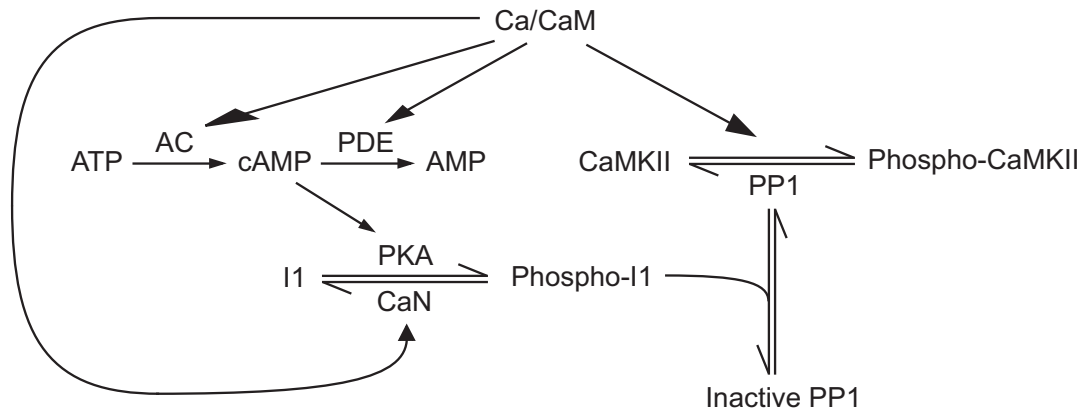


Figure S1: **PP1 regulation.** (A) A schematic reaction diagram demonstrating two mechanisms of Ca/CaM-dependent PP1 regulation. CaM directly activates CaN, which increases PP1 activity by dephosphorylating I1. CaM also acts indirectly through the cAMP pathway by controlling the activity of CaM-dependent ACs and PDEs. This pathway decreases PP1 activity through PKA-dependent phosphorylation of I1.

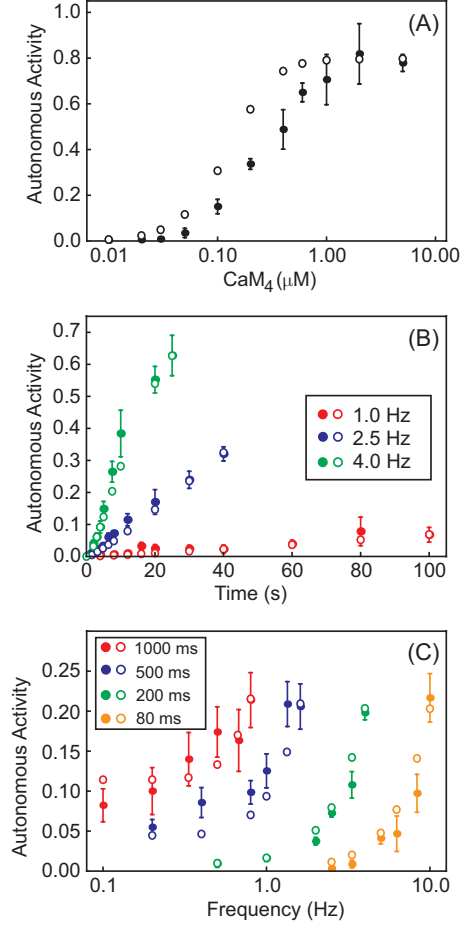


Figure S2: **Validation of the model dynamics.** The model is used to reproduce the results of Ref. (3). Experimental results are labeled by closed circles and error bars, simulation results are labeled with open circles. Autonomous activity is defined relative to the maximum $\text{Ca}^{2+}/\text{CaM}$ -stimulated activity of an identically treated sample. (A) CaMKII autonomy as a function of saturated CaM. CaMKII was exposed to a continuous 6-second stimulation with varying concentrations of saturated CaM. The model reproduces the experimental Hill coefficient but slightly underestimates the measured EC_{50} . (B) CaMKII autonomy as a function of time. CaMKII was exposed to one hundred, 200 ms pulses of $0.1 \mu\text{M}$ CaM₄ at one of three different frequencies, as indicated in the figure legend. (C) CaMKII autonomy as a function of frequency. CaMKII was exposed to $0.1 \mu\text{M}$ CaM₄ pulses of different durations and frequencies, with the total number of pulses adjusted to keep total exposure time at 6 seconds. The curves are color coded according to pulse duration, as indicated in the figure legend. Parameters: $\text{CaMKII}_{\text{tot}} = 0.005 \mu\text{M}$, $k_{\text{on},u} = 4.0 \mu\text{M}^{-1} \text{s}^{-1}$, $k_{\text{off},u} = 0.66 \text{s}^{-1}$, $r_1 = 1.0 \text{s}^{-1}$.

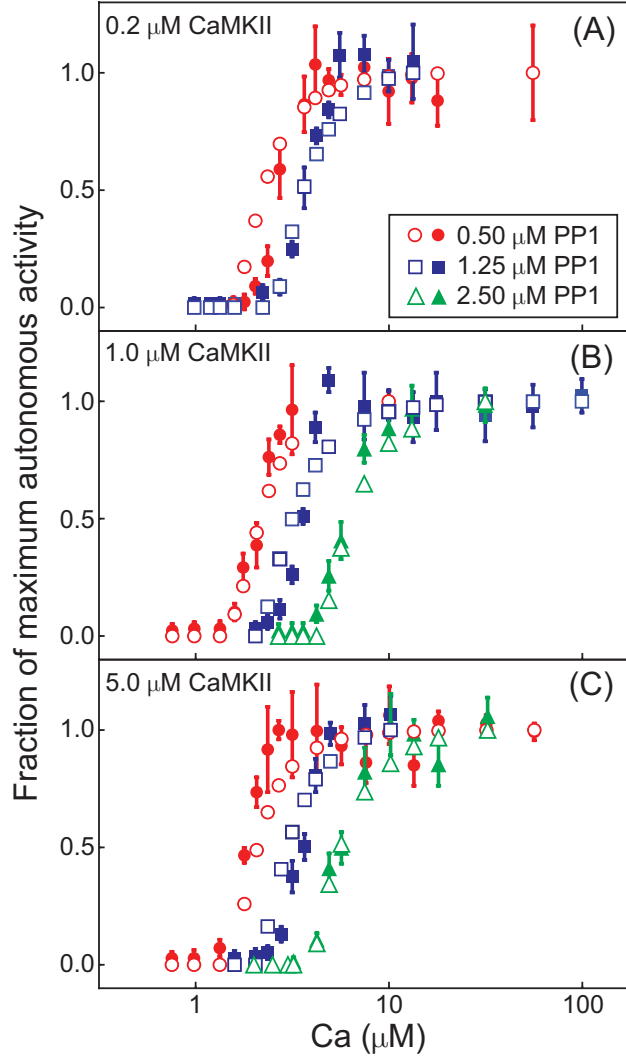


Figure S3: **Validation of steady state properties.** The model is used to reproduce the results of Ref. (4). Experimental results are labeled with closed symbols and error bars, model results are labeled with open symbols. Each plot shows the fraction of maximal autonomous activity as a function of Ca^{2+} as the total concentrations of CaMKII and PP1 are varied. (A) $0.2 \mu\text{M}$ CaMKII, (B) $1.0 \mu\text{M}$ CaMKII, (C) $5 \mu\text{M}$ CaMKII. The curves are color coded according to the concentration of PP1, as indicated in the legend. The fitted values of E_{th} were (A) $0.05 \mu\text{M}$, (B) $0.15 \mu\text{M}$, and (C) $0.75 \mu\text{M}$. Other parameters: $\text{CaM}_{\text{tot}} = 50 \mu\text{M}$, $r_1 = 1 \text{ s}^{-1}$, $r_3 = r_4 = 0$ (according to (4)), $K_0 = 10 \mu\text{M}$, $K_1 = 0.1 \mu\text{M}$, $k_{\text{on},u} = 3 \mu\text{M}^{-1} \text{ s}^{-1}$, and $k_{\text{on},p} = 0.3 \mu\text{M}^{-1} \text{ s}^{-1}$.

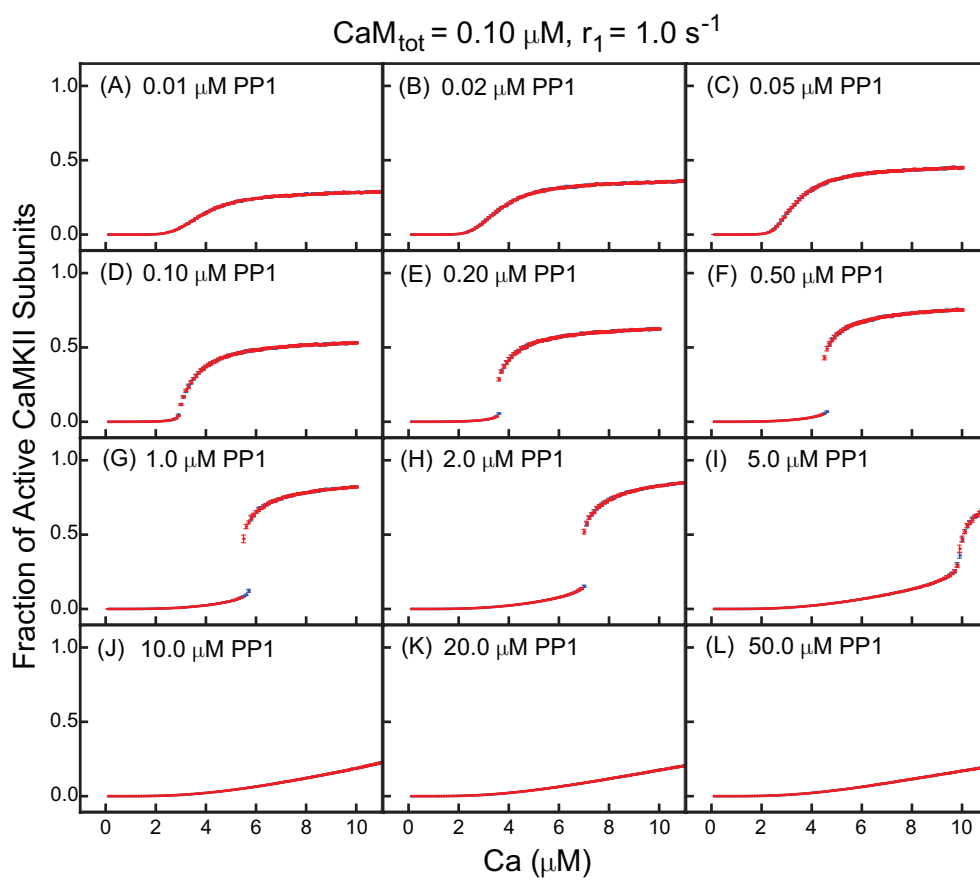


Figure S4: **Steady state activity curves.** Same as Fig. 6 but for $\text{CaM}_{\text{tot}} = 0.1 \mu\text{M}$ and $r_1 = 1 \text{ s}^{-1}$.

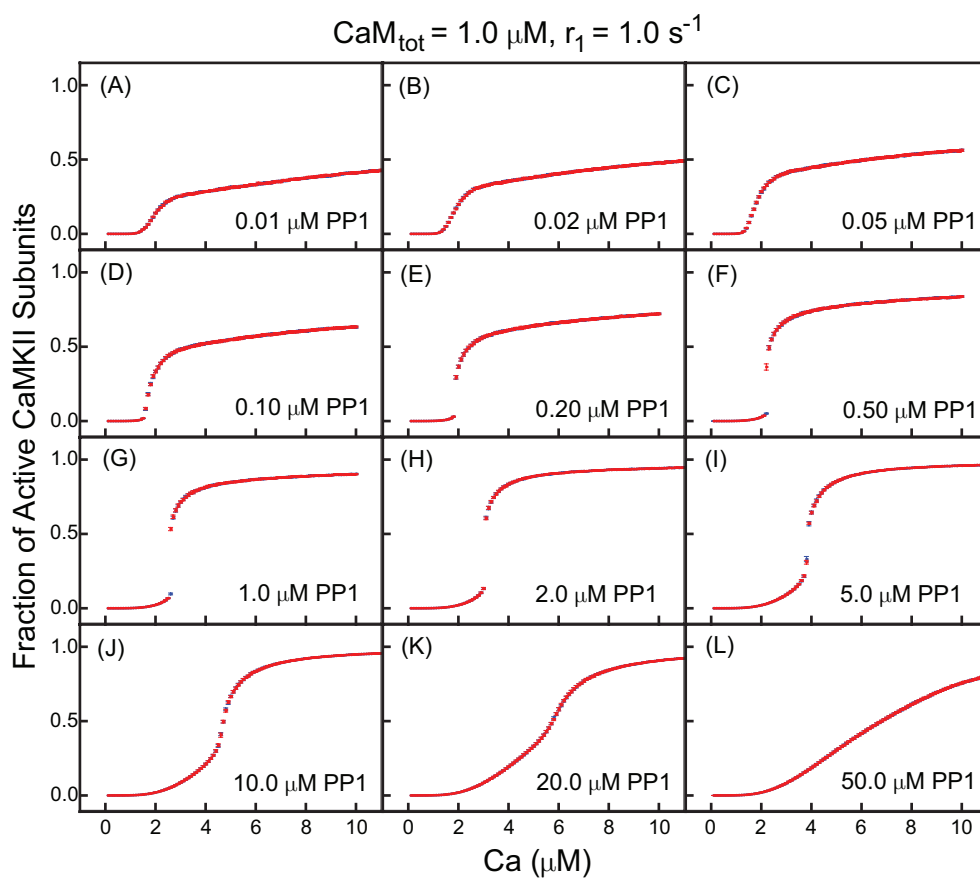


Figure S5: **Steady state activity curves.** Same as Fig. 6 but for $\text{CaM}_{\text{tot}} = 1 \mu\text{M}$ and $r_1 = 1 \text{ s}^{-1}$.

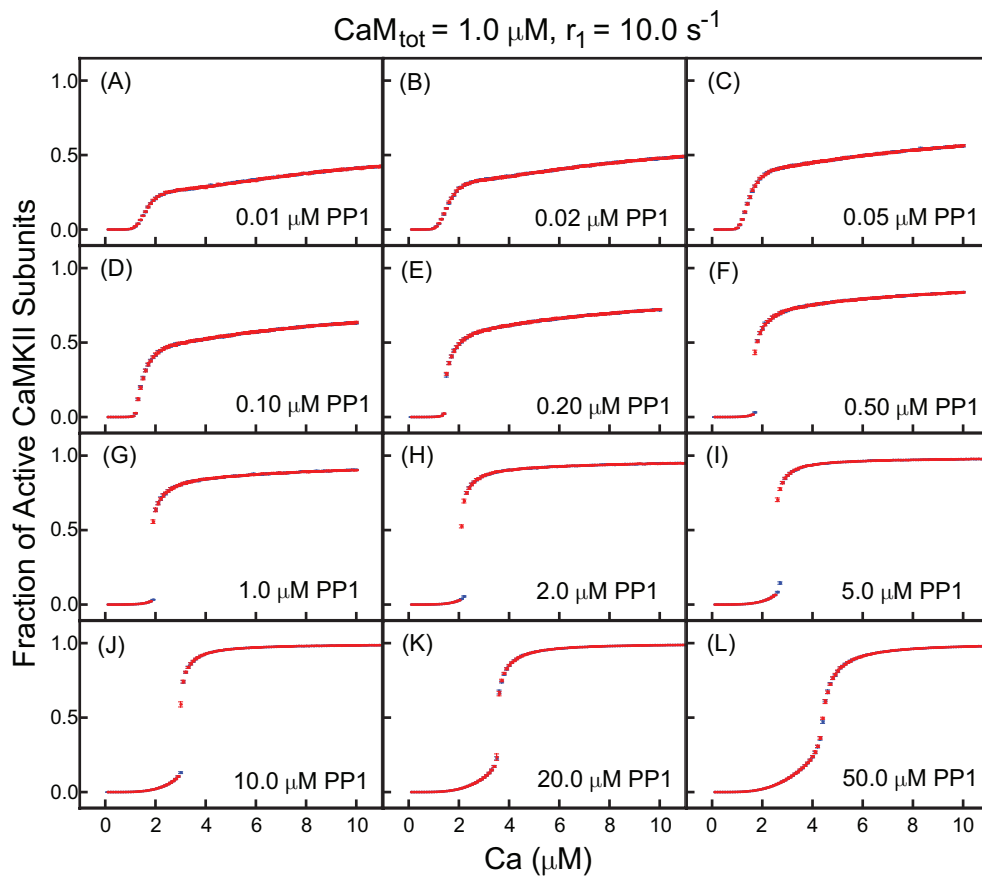


Figure S6: **Steady state activity curves.** Same as Fig. 6 but for $\text{CaM}_{\text{tot}} = 1 \mu\text{M}$ and $r_1 = 10 \text{ s}^{-1}$.

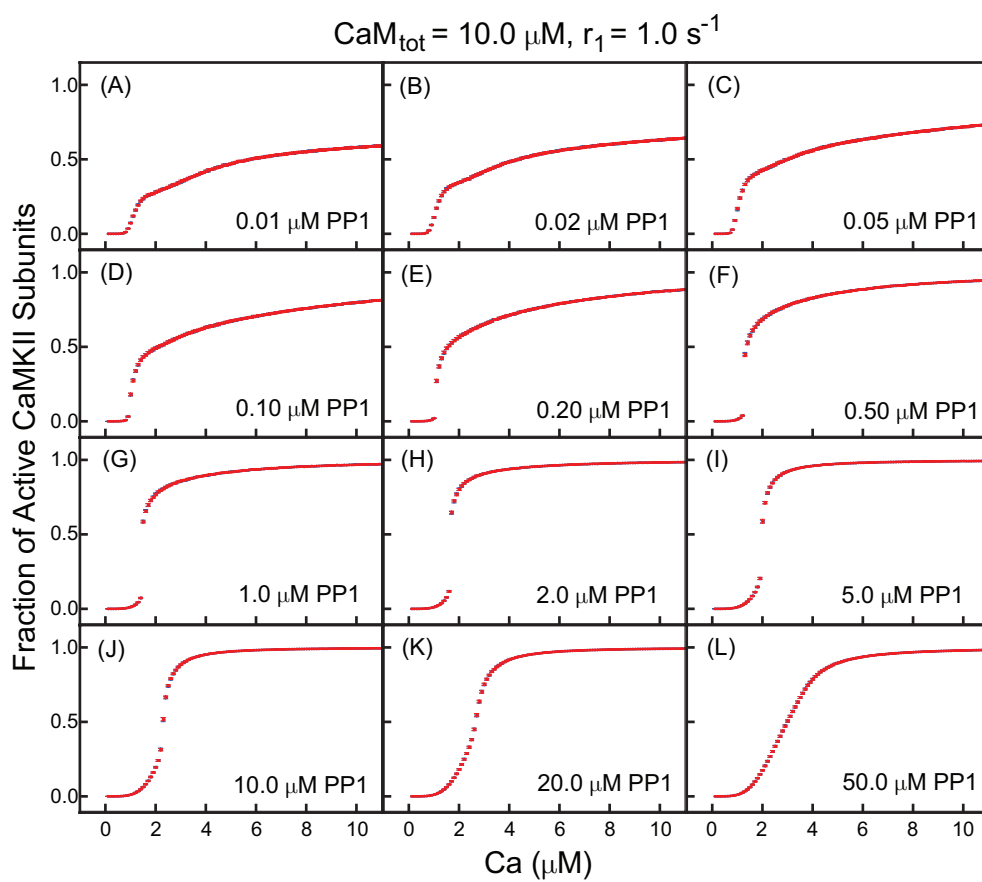


Figure S7: **Steady state activity curves.** Same as Fig. 6 but for $\text{CaM}_{\text{tot}} = 10 \mu\text{M}$ and $r_1 = 1 \text{ s}^{-1}$.

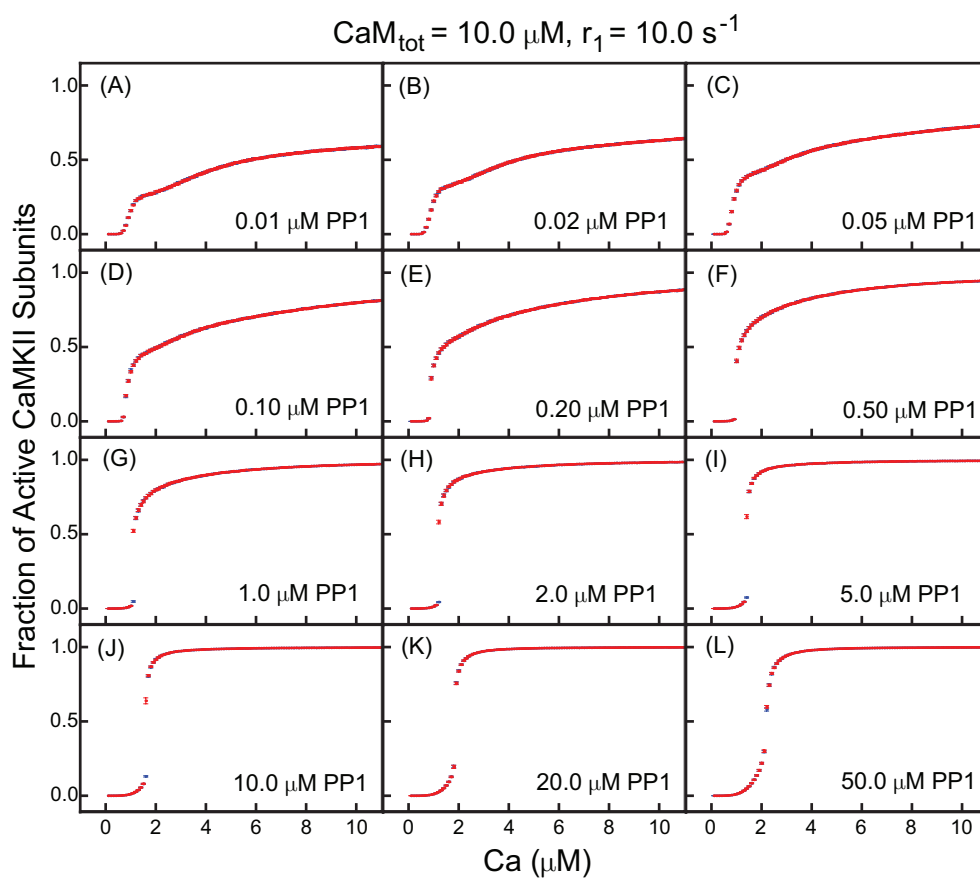


Figure S8: **Steady state activity curves.** Same as Fig. 6 but for $\text{CaM}_{\text{tot}} = 10 \mu\text{M}$ and $r_1 = 10 \text{ s}^{-1}$.

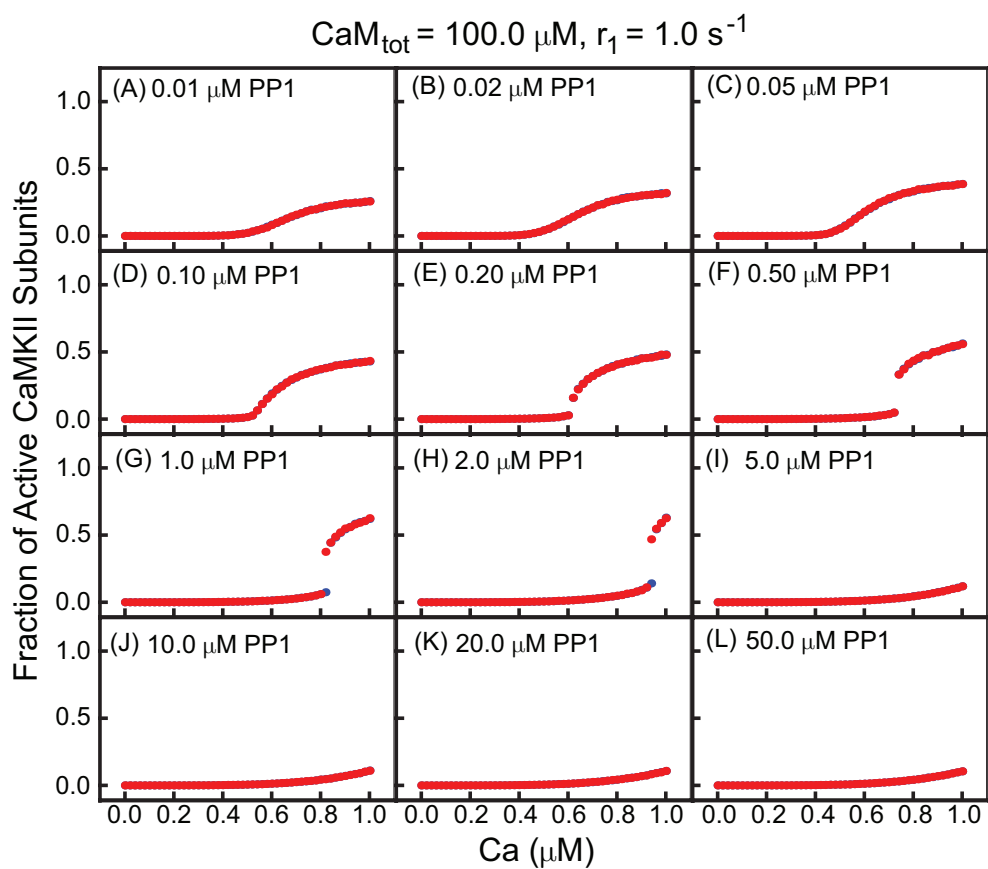


Figure S9: **Steady state activity curves.** Same as Fig. 6 but for $\text{CaM}_{\text{tot}} = 100 \mu\text{M}$ and $r_1 = 1 \text{ s}^{-1}$. Note that the x-axis is expanded compared to Fig. 6, to show the region near the origin.

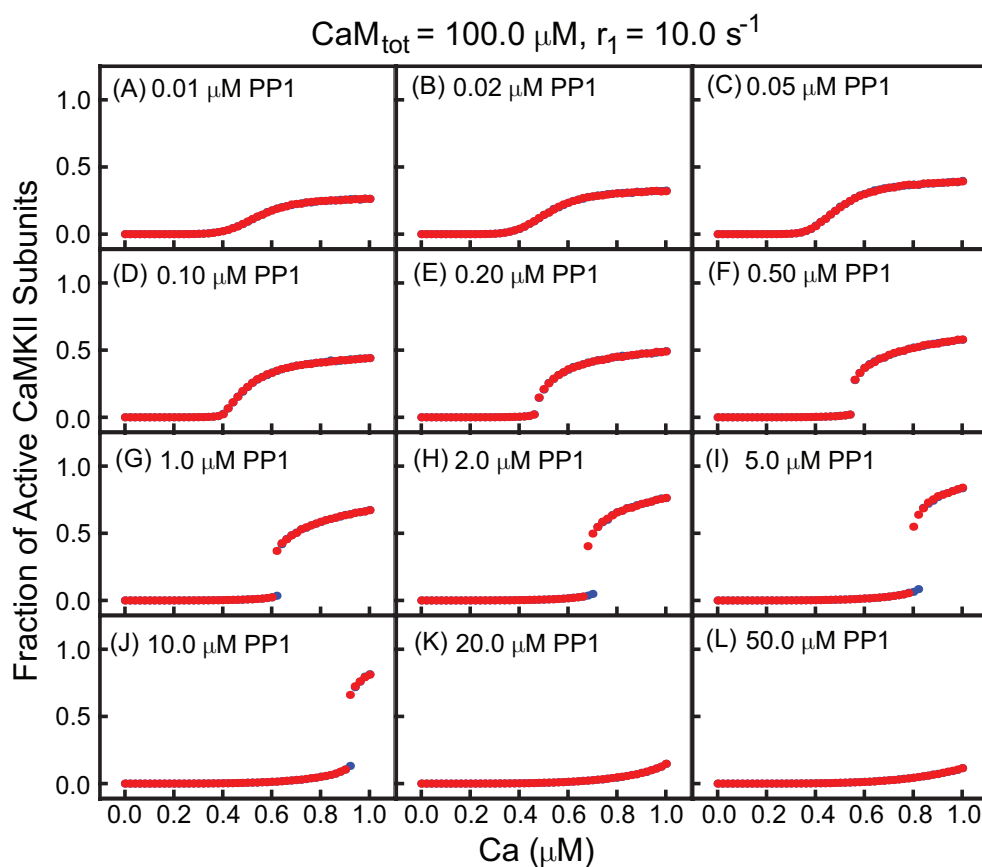


Figure S10: **Steady state activity curves.** Same as Fig. 6 but for $\text{CaM}_{\text{tot}} = 100 \mu\text{M}$ and $r_1 = 10 \text{ s}^{-1}$. Note that the x-axis is expanded compared to Fig. 6, to show the region near the origin.

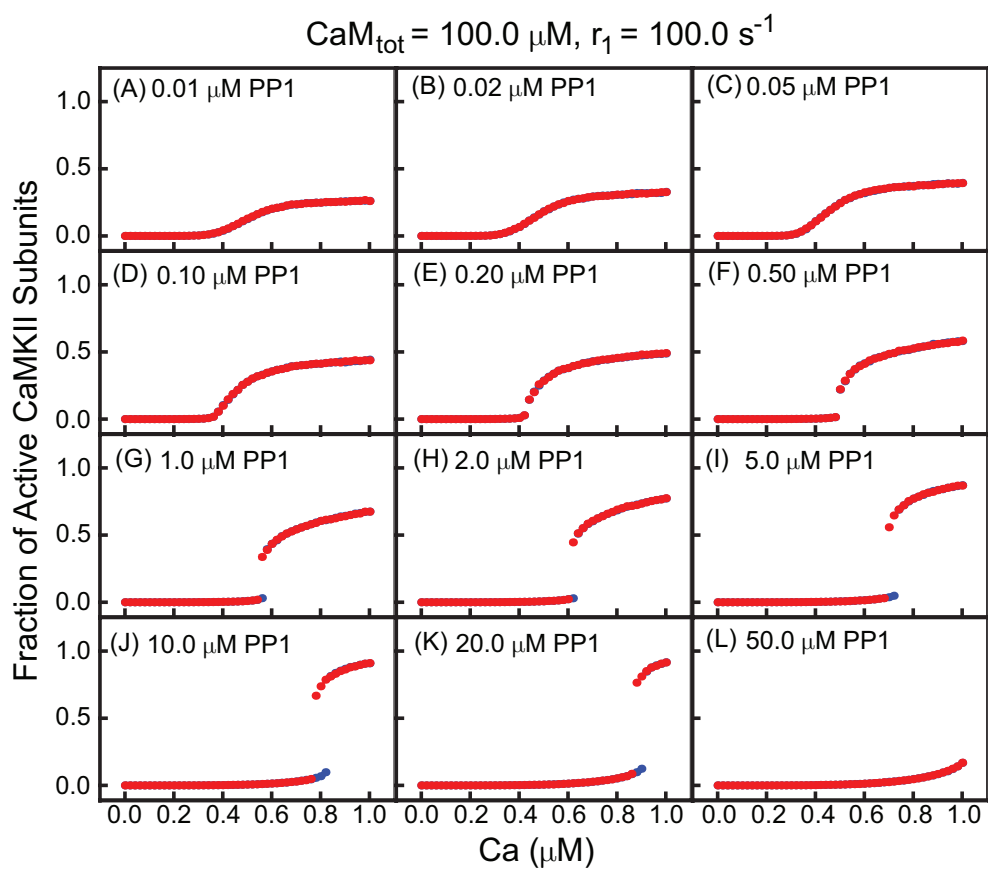


Figure S11: **Steady state activity curves.** Same as Fig. 6 but for $\text{CaM}_{\text{tot}} = 100 \mu\text{M}$ and $r_1 = 100 \text{ s}^{-1}$. Note that the x-axis is expanded compared to Fig. 6, to show the region near the origin.

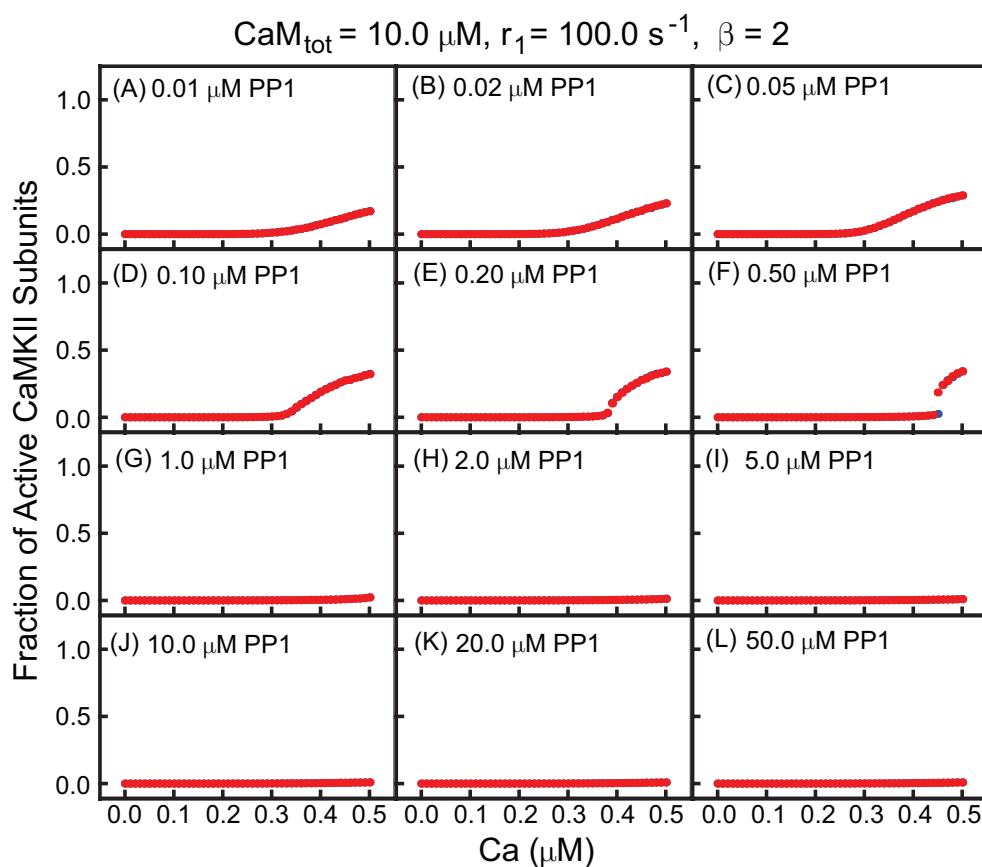


Figure S12: **Steady state activity curves with increased calcium-CaM affinity.** Same as Fig. 6 but for $\text{CaM}_{\text{tot}} = 10 \mu\text{M}$, $r_1 = 100 \text{ s}^{-1}$, and $\beta = 2$. Note that the x-axis is expanded compared to Fig. 6, to show the region near the origin.

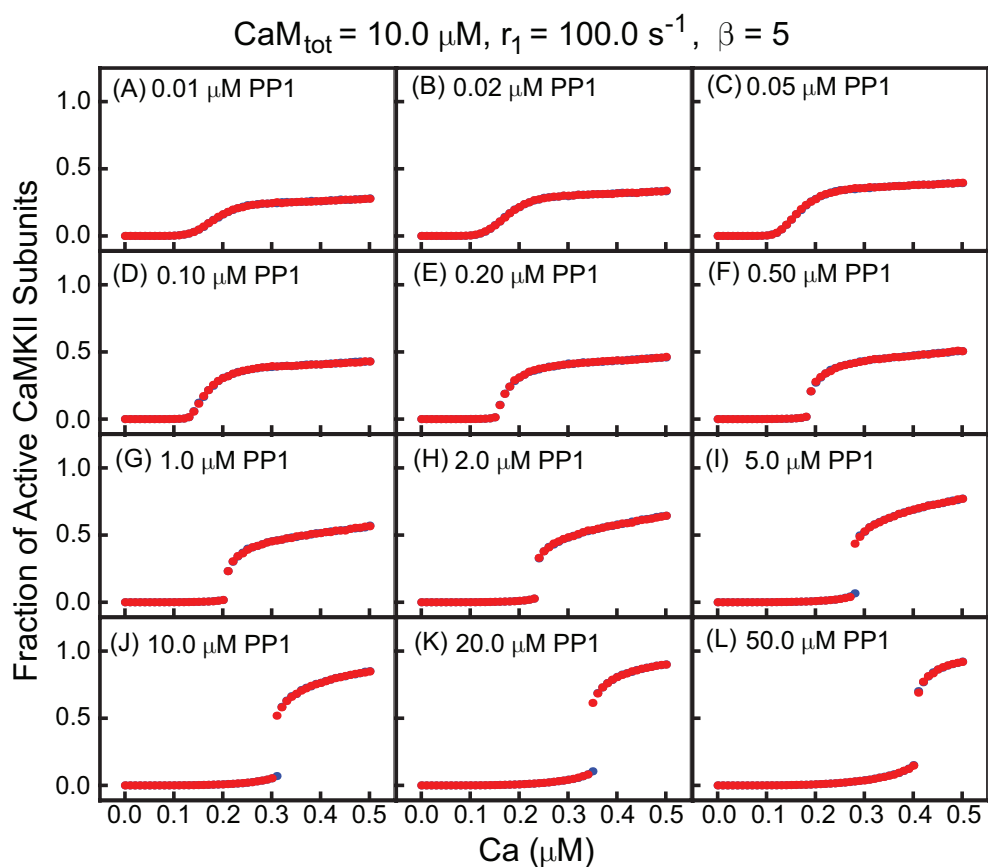


Figure S13: **Steady state activity curves with increased calcium-CaM affinity.** Same as Fig. 6 but for $\text{CaM}_{\text{tot}} = 10 \mu\text{M}$, $r_1 = 100 \text{ s}^{-1}$, and $\beta = 5$. Note that the x-axis is expanded compared to Fig. 6, to show the region near the origin.

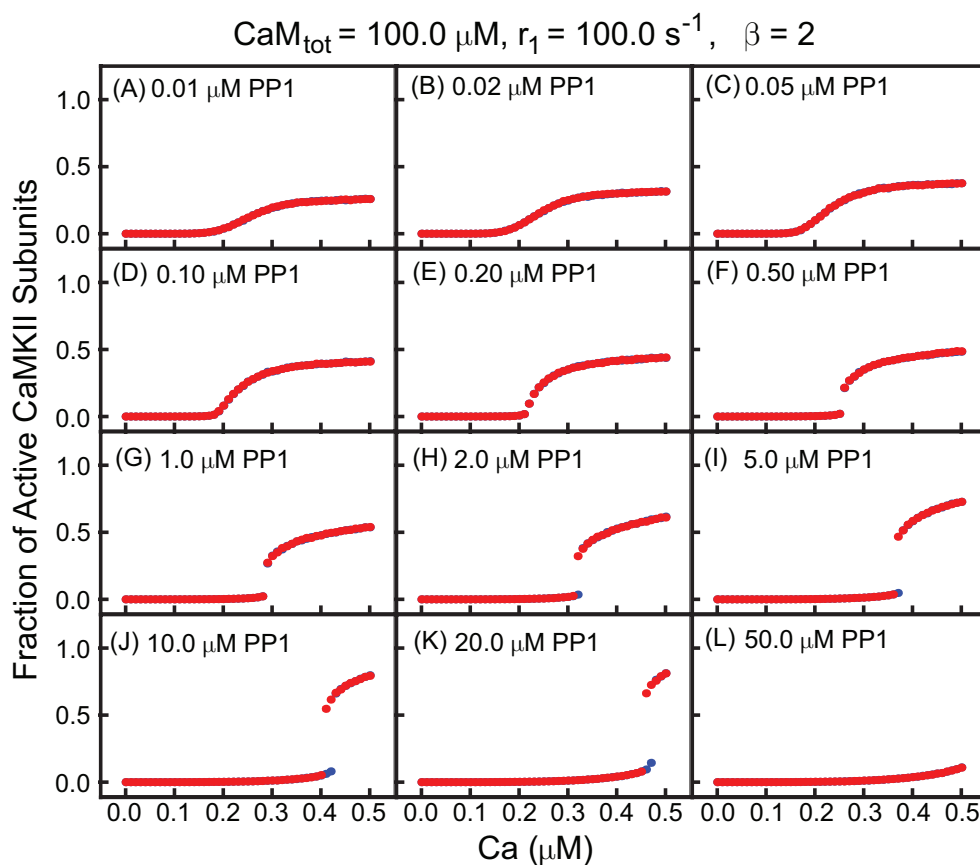


Figure S14: **Steady state activity curves with increased calcium-CaM affinity.** Same as Fig. 6 but for $\text{CaM}_{\text{tot}} = 100 \mu\text{M}$, $r_1 = 100 \text{ s}^{-1}$, and $\beta = 2$. Note that the x-axis is expanded compared to Fig. 6, to show the region near the origin.

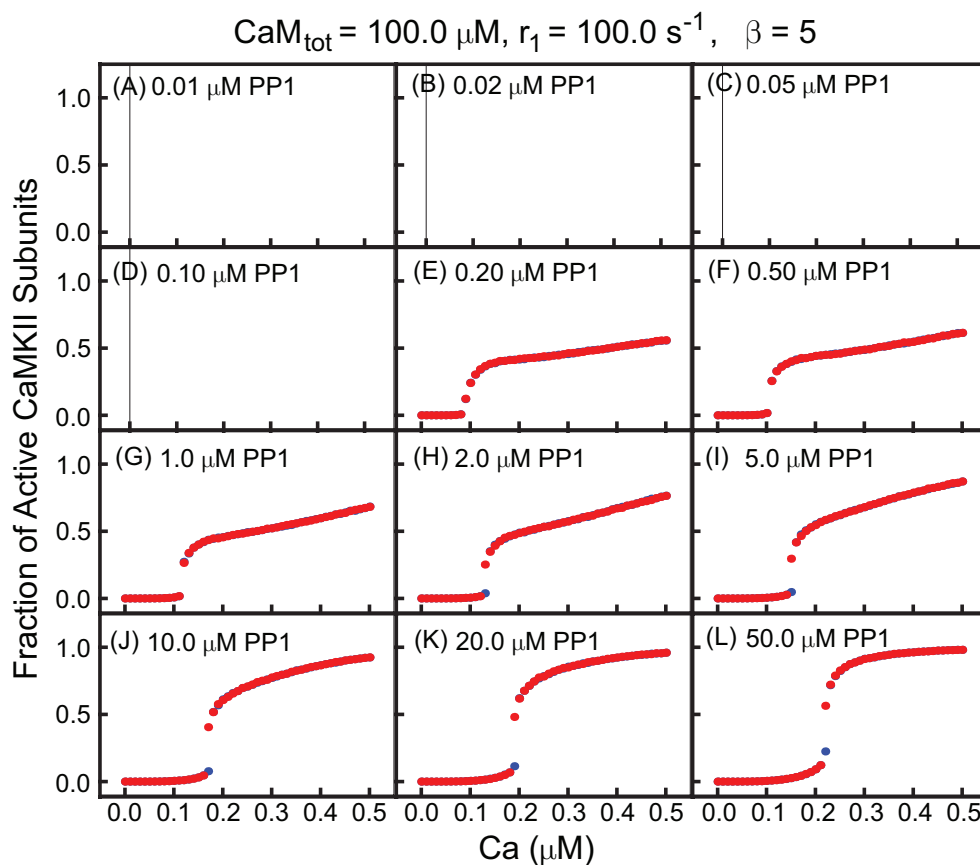


Figure S15: **Steady state activity curves with increased calcium-CaM affinity.** Same as Fig. 6 but for $\text{CaM}_{\text{tot}} = 100 \mu\text{M}$, $r_1 = 100 \text{ s}^{-1}$, and $\beta = 5$. Note that the x-axis is expanded compared to Fig. 6, to show the region near the origin.

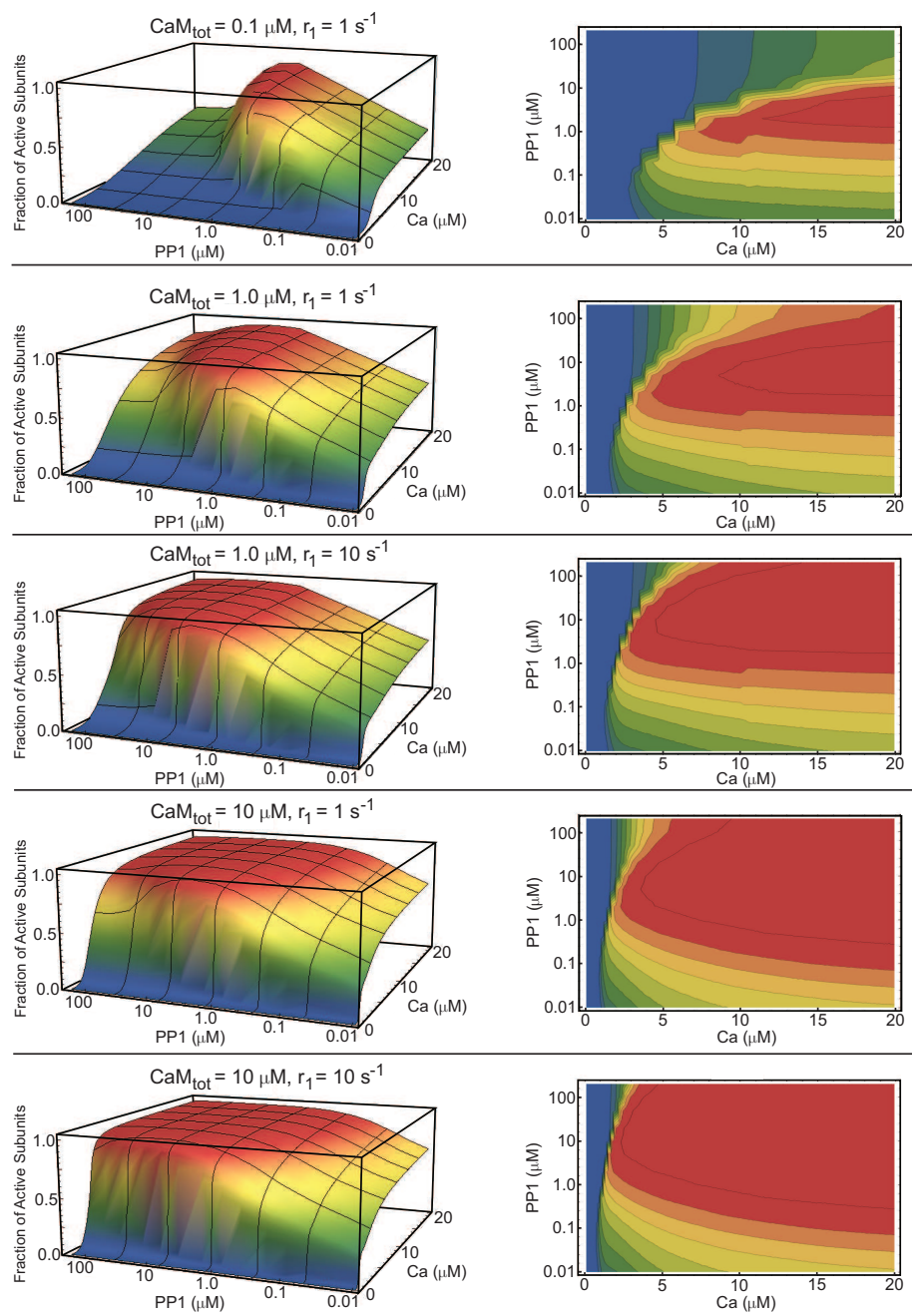


Figure S16: **CaMKII activity phase diagrams.** Same as Fig. 7, but for the activity curves shown in Figs. S4-S8.

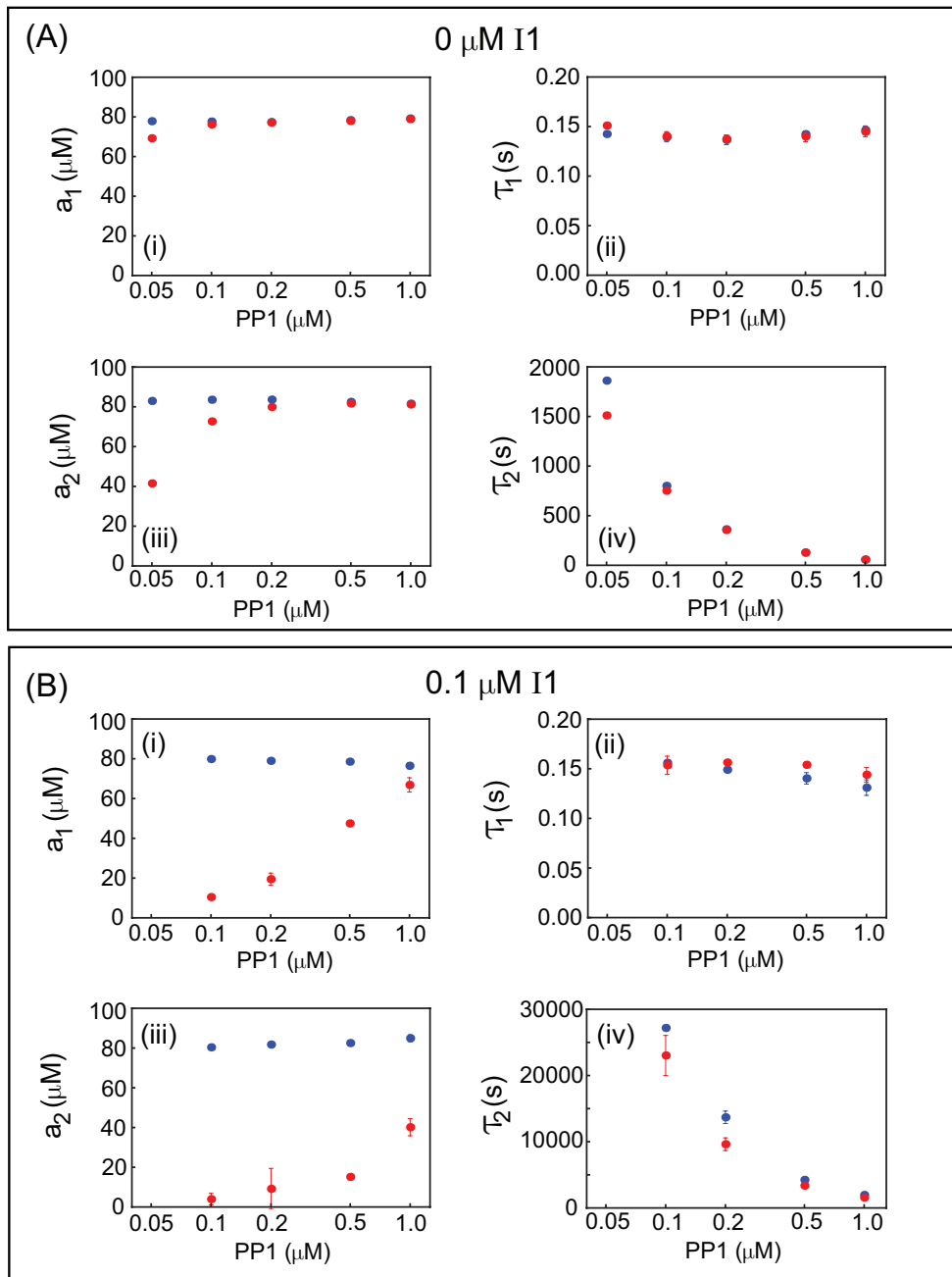


Figure S17: **Characterization of response to LTP protocols.** Same as Fig. 10, but for other values of I_{tot} .

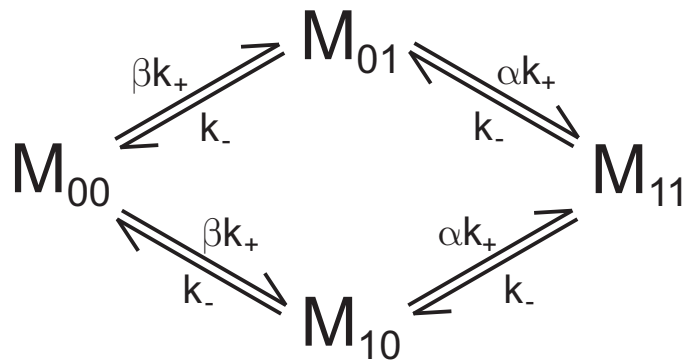


Figure S18: **Reaction scheme for dimer holoenzyme in absence of autophosphorylation.** The dimer holoenzyme can be described by four states depending on which subunit is inactive (0) and which is CaM-bound (1). The cooperative model considered in the Supporting Text assumes that all cooperativity arises from changes in the on-rate. CaM binding to the fully inhibited dimer occurs with an on-rate βk_+ , while CaM binding to the partially active dimer occurs with an on-rate of αk_+ . The non-cooperative limit occurs when $\alpha = \beta = 1$. In order to ensure a finite effective dissociation constant in the fully cooperative limit, $\alpha \rightarrow \infty$, we set $\beta = 1/\alpha$. See the Supporting Text for details.

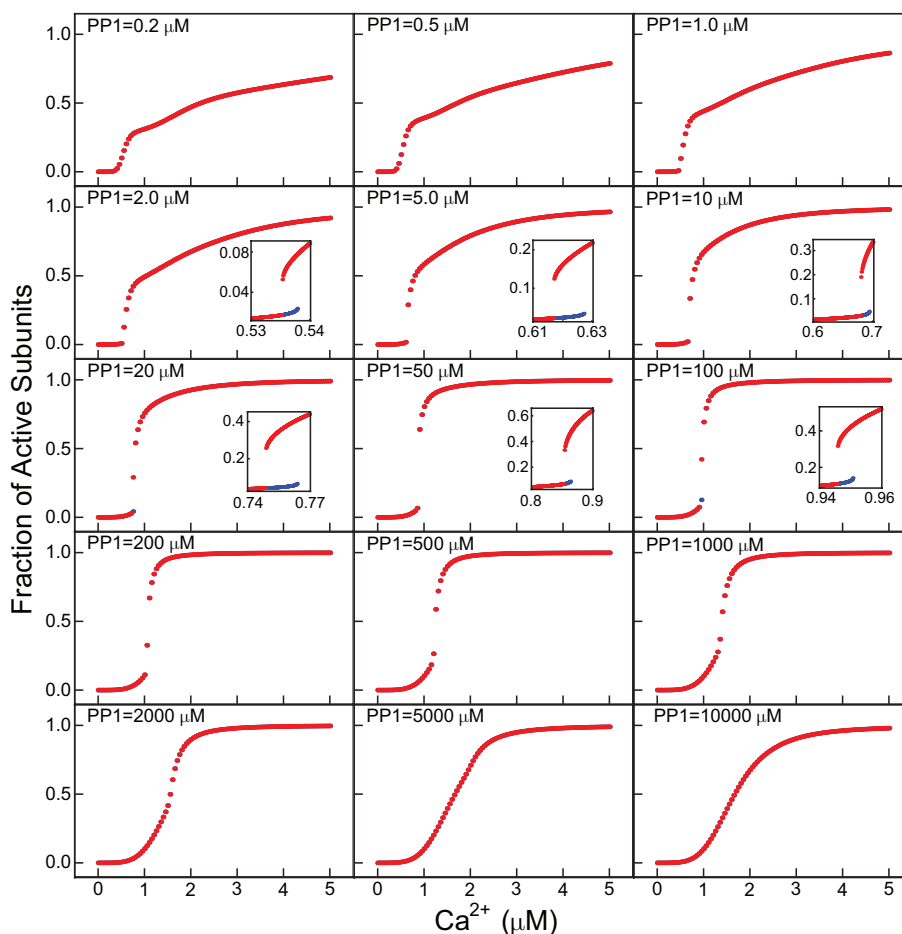


Figure S19: **Steady-state activation curves for the non-cooperative dimer holoenzyme.** CaMKII steady-state activation is plotted as a function of calcium for many values of PP1. A comparison of this figure with Fig. 6 shows that the dimer model is able to recapitulate the full range of behaviors seen in the hexamer. Blue data points are obtained as calcium is incremented from low to high values; red data points are obtained as calcium is decremented from high to low values. The insets show tiny regions of bistability which characterize step-like activation curves. Results obtained with standard parameters and the fast set of autophosphorylation rates ($r_1 = 10 \text{ s}^{-1}$, etc), while $\text{CaMKII} = 200 \text{ } \mu\text{M}$ and $\text{CaM} = 100 \text{ } \mu\text{M}$ for reasons discussed in the supporting text.

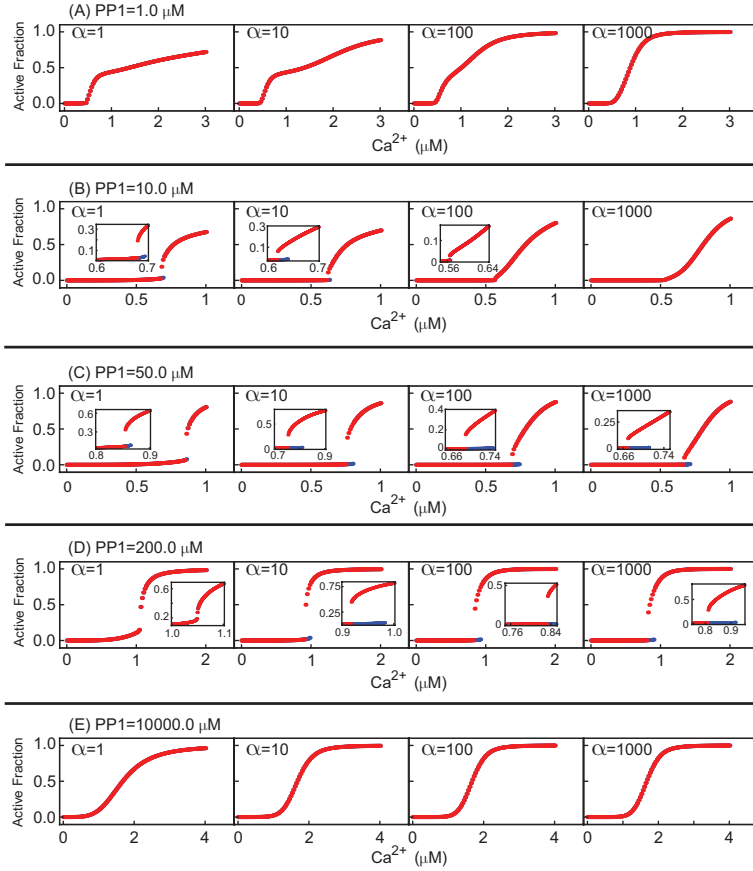


Figure S20: **The effect of cooperative CaM binding on steady state CaMKII activation curves.** These examples illustrate the full range of possible changes which occur as cooperativity is increased. The left-most curve in each row reproduces a non-cooperative curve from Fig. S19, while the other three curves show the effect of increasing cooperativity. Cooperativity is turned on by increasing α in powers of 10 up to 1000. (We continued this progression up to $\alpha = 10^6$ to verify a limiting behavior was attained at $\alpha = 1000$.) (A) Increasing cooperativity converts a laser-like activation curve to a Hill-like activation curve. (B) Increasing cooperativity converts a step-like activation with a narrow region of bistability into a laser-like activation. (C) Increasing cooperativity modifies the exact shape of the step-like activation curve but does not eliminate the narrow region of bistability. (D) Increasing cooperativity converts a very steep Hill-like curve into a step-like curve with a narrow region of bistability. (E) Increasing cooperativity increases the effective Hill coefficient of a Hill-like activation curve. Insets show expanded views of the regions of bistability, except the first inset in (D), which shows that no bistability is evident when calcium is incremented in steps of 1 nM. Blue curves: calcium incremented from low to high values. Red curves: calcium incremented from high to low values. All parameters as in Fig. S19.

References

1. Michalski, P. J., and L. M. Loew, 2012. CaMKII activation and dynamics are independent of the holoenzyme structure: an infinite subunit holoenzyme approximation. *Phys. Biol.* 9:036010.
2. Slepchenko, B. M., J. C. Schaff, I. Macara, and L. M. Loew, 2003. Quantitative cell biology with the Virtual Cell. *Trends Cell Biol.* 13:570 – 576.
3. De Koninck, P., and H. Schulman, 1998. Sensitivity of CaM kinase II to the frequency of Ca^{2+} oscillations. *Science* 279:227 – 230.
4. Bradshaw, J. M., Y. Kubota, T. Meyer, and H. Schulman, 2003. An ultrasensitive Ca^{2+} /calmodulin-dependent protein kinase II-protein phosphatase 1 switch facilitates specificity in postsynaptic calcium signaling. *PNAS* 100:10512 – 10517.
5. Chao, L. H., P. Pellicena, S. Deindl, L. A. Barclay, H. Schulman, and J. Kuriyan, 2010. Intersubunit capture of regulatory segments is a component of cooperative CaMKII activation. *Nat. Struct. Mol. Biol.* 17:264 – 272.
6. Rosenberg, O. S., S. Deindl, R.-J. Sung, A. C. Nairn, and J. Kuriyan, 2005. Structure of the autoinhibited kinase domain of CaMKII and SAXS analysis of the holoenzyme. *Cell* 123:849 – 860.
7. Thaler, C., S. V. Koushik, H. L. Puhl III, P. S. Blank, and S. S. Vogel, 2009. Structural rearrangement of CaMKII α catalytic domains encodes activation. *PNAS* 106:6369 – 6374.
8. Linse, S., A. Helmersson, and S. Forsén, 1991. Calcium binding to calmodulin and its globular domains. *J. Biol. Chem.* 266:8050 – 8054.
9. Meyer, T., P. I. Hanson, L. Stryer, and H. Schulman, 1992. Calmodulin trapping by calcium-calmodulin-dependent protein kinase. *Science* 256:1199 – 1202.
10. Gaertner, T. R., S. J. Kolodziej, D. Wang, R. Kobayashi, J. M. Koomen, J. K. Stoops, and M. N. Waxham, 2004. Comparative analyses of the three-dimensional structures and enzymatic properties of α , β , γ , and δ isoforms of Ca^{2+} -calmodulin-dependent protein kinase II. *J. Biol. Chem.* 279:12484 – 12494.
11. Lengyel, I., S. Fieuw-Makaroff, A. L. Hall, A. T. R. Sim, J. A. P. Rostas, and P. R. Dunkley, 2000. Modulation of the phosphorylation and activity of calcium/calmodulin-dependent protein kinase II by zinc. *J. Neurochem.* 75:594 – 605.
12. Colbran, R. J., 1993. Inactivation of Ca^{2+} /calmodulin-dependent protein kinase II by basal autophosphorylation. *J. Biol. Chem.* 268:7163 – 7170.

13. Endo, S., X. Zhou, J. Connor, B. Wang, and S. Shenolikar, 1996. Multiple structural elements define the specificity of recombinant human inhibitor-1 as a protein phosphatase-1 inhibitor. *Biochemistry* 35:5220 – 5228.
14. Graupner, M., and N. Brunel, 2007. STDP in a bistable synapse model based on CaMKII and associated signaling pathways. *PLoS Comput. Biol.* 3:e221.